

Ionization by Electron Impact in CO, N₂, NO, and O₂

HOMER D. HAGSTRUM

Bell Telephone Laboratories, Murray Hill, New Jersey

Ionization by electron impact in diatomic gases has been studied in this work with a mass spectrometer designed to measure m/e , appearance potential, and initial kinetic energy for each ion observed. Results have been obtained for the gases CO, N₂, NO, and O₂ with some confirmatory work in H₂. Discussion is included of the nature and identification of dissociative ionization processes and of the retarding potential and appearance potential measurements. Values of important quantities such as the dissociation energies of CO, N₂, and NO; the sublimation energy of C; the electron affinity of O; and the excitation energy of O⁻ are determined again by electron impact in this work.

I. INTRODUCTION

OF particular interest in the study of electron collisions in diatomic gases are the ionization processes in which the molecule dissociates. To specify completely each dissociative ionization process we must know (1) the identity of the atomic fragments as to states of ionization and excitation, (2) their distribution in initial kinetic energy, and (3) the onset potential for fragments of known initial kinetic energy. Thus, it is clear that the electron collision experiment should be designed so as to permit the measurement of (1) m/e , (2) appearance potential, and (3) kinetic energy of each ion observed. In mass spectrometric investigations generally only the first and second of these quantities have been determined, and in Lozier's retarding potential method¹⁻⁴ only the second and third.

The use by Bleakney⁵ of retarding potentials in the ion source of a mass spectrometer to differentiate ions formed with negligible kinetic energy from those formed with appreciable kinetic energy in hydrogen represents the first attempt to determine m/e , appearance potential, and initial kinetic energy in the same experiment. Since then, other methods of accomplishing this have been investigated. Hagstrum and Tate⁶ studied the effect of initial kinetic energy and velocity dispersion in the mass analyzer on the so-called ion peak shape. Distinguishable types of initial kinetic energy distributions were observed and interpreted, and measurements made of the relation of appearance potential to initial energy. Berry⁷ has used the discrimination at the exit slit of the mass analyzer to determine the initial distribution in the component of velocity along the length of the slit. No attempt to determine the relation between appearance potential and kinetic energy was made, however. After the successful use of retarding

potentials following mass analysis in the study of spontaneous dissociation of metastable ions in transit through the mass spectrometer,⁸ Fox and Hipple⁹ have suggested the use of this method to determine initial kinetic energies. These investigators studied the ionization of *n*-butane in this way and showed that ions of low mass may have initial kinetic energies of several electron-volts. Here again, no measurement was made of appearance potential and kinetic energy at the same time.

In the present work the measurement of kinetic energy by retardation following mass analysis in a mass spectrometer has been studied further. For this purpose an instrument incorporating a 90° magnetic analyzer and electrostatic ion lenses was constructed. With it, determinations of m/e , appearance potential, and initial kinetic energy have been made for each ion observed from simple and dissociative ionization processes in CO, N₂, NO, and O₂. Some work to test the method was done in H₂.

In this paper the nature of the dissociative ionization process in diatomic gases and how, in detail, it is to be identified are first discussed (Sec. II). Following a brief description of the experimental apparatus (Sec. III), the retarding potential and appearance potential measurements are examined (Secs. IV and V). Next, the experimental results for simple and dissociative ionization in CO, N₂, NO, and O₂ are presented and conclusions from them drawn (Secs. VI and VII). Singled out for investigation in more detail are the processes yielding O⁺ in CO and NO (Sec. VIII) and those yielding O⁻ in CO, NO, and O₂ by dissociative electron capture (Sec. IX). In the final four sections of the paper are discussed a number of important energies derivable from the electron impact results. These are the dissociation energy of CO and sublimation energy of C (Sec. X), the dissociation energies of N₂ and NO (Sec. XI), the electron affinity of O (Sec. XII), and the

¹ W. W. Lozier, Phys. Rev. **36**, 1285 (1930) [H₂].

² W. W. Lozier, Phys. Rev. **44**, 575 (1933); **45**, 840 (1934) [N₂].

³ W. W. Lozier, Phys. Rev. **46**, 268 (1934) [CO, O₂].

⁴ E. E. Hanson, Phys. Rev. **51**, 86 (1937) [NO].

⁵ W. Bleakney, Phys. Rev. **35**, 1180 (1930).

⁶ H. D. Hagstrum and J. T. Tate, Phys. Rev. **59**, 354 (1941).

⁷ C. E. Berry, Phys. Rev. **78**, 597 (1950); see H. W. Washburn and C. E. Berry, Phys. Rev. **70**, 559 (1946).

⁸ Hipple, Fox, and Condon, Phys. Rev. **69**, 347 (1946).

⁹ R. E. Fox and J. A. Hipple, Rev. Sci. Instr. **19**, 462 (1948); J. A. Hipple, J. Phys. and Colloid Chem. **52**, 456 (1948).

TABLE I. Definitions of symbols.

e^-	Electron
X, Y	Atoms
X^+, Y^-	Atomic ions
XY	Diatomic molecule
XY^+, XY^-	Diatomic molecular ions
$X^+(XY)$	X^+ ion derived from XY by electron impact
$m(X)$	Mass of X
$E_k(e^-), E_k(X^+)$	Kinetic energies of e^- and X^+ , respectively
$I(X)$	Ionization potential of X
$EA(X)$	Electron affinity of X
$E_e(X)$	Electronic excitation energy of X
$D(XY)$	Dissociation energy of XY
$L(X)$	Sublimation energy of X
$\Delta E_k(e^-)$	Loss in kinetic energy of bombarding electron
$A_k(X^+), A_k$	Appearance potential of X^+ of kinetic energy $E_k(X^+)$
$A_0(X^+), A_0$	Appearance potential of X^+ of zero kinetic energy
$A(X^+)_{XY}$	Appearance potential (without reference to kinetic energy) of X^+ ions from the molecule XY
V_{NP}	Retarding potential applied in retardation chamber
V_P	Voltage of electrode P <i>re</i> : source of ions
I_P	Total current to electrode P
I^+	Positive ion current entering retardation chamber
γ	Electron current ejected from electrodes per unit positive ion current
f_P	Fraction of I^+ reaching electrode P

energy level of the excited state of O^- (Sec. XIII). Definitions of symbols used are given in Table I.

II. THE DISSOCIATIVE IONIZATION PROCESS

In diatomic gases like CO , N_2 , NO , and O_2 there are three types of dissociative ionization possible. These are listed in Table II. Assignment of each ion observed in the mass spectrum to a specific process can be made with the help of the appearance potential for ions having zero initial kinetic energy.^{3,6,10} Appearance of a positive ion alone at a given minimum electron energy indicates the process in which it is formed to be type (A) (Table II). Simultaneous appearance of a positive and a negative ion indicates process (B).¹¹ Appearance of the negative ion at electron energies so low that a positive ion cannot simultaneously be formed indicates process (C). The state of electronic excitation of the products is specified by intercomparison of the appearance potentials for several ions observed in the same gas or a related gas, in the manner to be discussed presently.

The kinetic energy of the products of dissociative ionization is fixed by the electronic transition induced in the molecule at electron impact. How this comes about is perhaps best described in terms of a potential energy diagram like that of Fig. 1. For a particular electronic transition the total kinetic energy of the dissociation products is seen to be the distance above the dissociation limit of the point on the upper potential

¹⁰ H. D. Hagstrum, *Phys. Rev.* **72**, 947 (1947).

¹¹ In fact, appearance of the negative ion at an electron energy near 20 eV in these gases of itself indicates process (B) even though the appearance of the positive ion is masked by the same ion from another process. A case in point is the process in O_2 commencing at 22.0 eV (Sec. V).

curve to which transition takes place. The distribution in kinetic energy of the products (curves 4 and 5 in Fig. 1) may be determined approximately by the reflection method,¹² in which the square of the ground-state vibrational eigenfunction is reflected in the upper potential curve onto the energy axis. Figure 1 indicates the fact, important for the proper interpretation of dissociative ionization processes, that quite different distributions in initial kinetic energy may occur depending on the position of the upper potential curve in the Franck-Condon region. Thus, transitions to curve 2 of Fig. 1 yield ions of initial kinetic energy including zero, whereas all ions from transitions to curve 3 possess appreciable initial kinetic energies. This is, in fact, the distinction first predicted theoretically by Condon¹³ for hydrogen and verified experimentally by Bleakney⁵ and Lozier.¹

The energy acquired by the molecule, which equals that lost by the bombarding electron, $\Delta E_k(e^-)$, is defined as the appearance potential $A_k(X^+)$ of X^+ ions of kinetic energy $E_k(X^+)$. For a process of type (A) (Table II), used here as an illustrative example, this potential is seen from Fig. 1 to be

$$A_k(X^+) = D(XY) + I(X) + E_e(X^+) + E_e(Y) + E_k(X^+) + E_k(Y).$$

The total kinetic energy divides between the fragments according to the law of conservation of momentum so that the ion kinetic energy in this case is

$$E_k(X^+) = [m(Y)/(m(X^+) + m(Y))][E_k(X^+) + E_k(Y)].$$

Thus, one has

$$A_k(X^+) = A_0(X^+) + [(m(X^+) + m(Y))/m(Y)]E_k(X^+).$$

In this expression

$$A_0(X^+) = D(XY) + I(X) + E_e(X^+) + E_e(Y)$$

is the energy level of the dissociation limit of the process (the horizontal asymptote of the upper potential curve) above the ground state of the molecule.¹⁴ The plot of

TABLE II. Types of dissociative ionization processes.

Type*	Process	A_0
(A)	$XY + e^- \rightarrow X^+ + Y + 2e^-$	$D(XY) + I(X) + E_e(X^+) + E_e(Y)$
(B)	$XY + e^- \rightarrow X^+ + Y^- + e^-$	$D(XY) + I(X) - EA(Y) + E_e(X^+) + E_e(Y^-)$
(C)	$XY + e^- \rightarrow X + Y^-$	$D(XY) - EA(Y) + E_e(X) + E_e(Y^-)$

* For heteronuclear molecules processes with X and Y interchanged are possible. These are indicated as types (A'), (B'), and (C'), respectively.

¹² Hagstrum and Tate (reference 6) discuss this application of the reflection method to dissociative ionization processes in more detail. Compare the use of the method in the interpretation of intensity distributions in absorption spectroscopy as discussed in G. Herzberg, *Spectra of Diatomic Molecules* (D. Van Nostrand Company, Inc., New York, 1950), second edition, p. 391 ff.

¹³ E. U. Condon, *Phys. Rev.* **35**, 658(A) (1930); see E. U. Condon and H. D. Smyth, *Proc. Natl. Acad. Sci. U. S. A.* **14**, 871 (1928), in which other critical potentials in molecular hydrogen are discussed.

¹⁴ Expressions for A_0 for each type of dissociative ionization process are included in Table II.

ion kinetic energy against appearance potential, two examples of which are shown in Fig. 2, is thus a straight line of slope $m(Y)/[m(X^+) + m(Y)]$ with intercept $A_0(X^+)$ on the $A_k(X^+)$ axis.¹⁵ The other curves in Fig. 2 are explained in the caption.

The determination of $A_0(X^+)$ either directly, if ions of zero initial energy are formed, or by simultaneous measurement of $E_k(X^+)$ and $A_k(X^+)$, if all ions possess kinetic energy, permits evaluation of the sum $D(XY) + I(X) + E_e(X^+) + E_e(Y)$.¹⁴ Since $I(X)$ and possible values of $E_e(X^+)$ and $E_e(Y)$ are known, one can calculate a series of possible values for $D(XY)$ if it is not known or is in doubt. Having calculated such a series

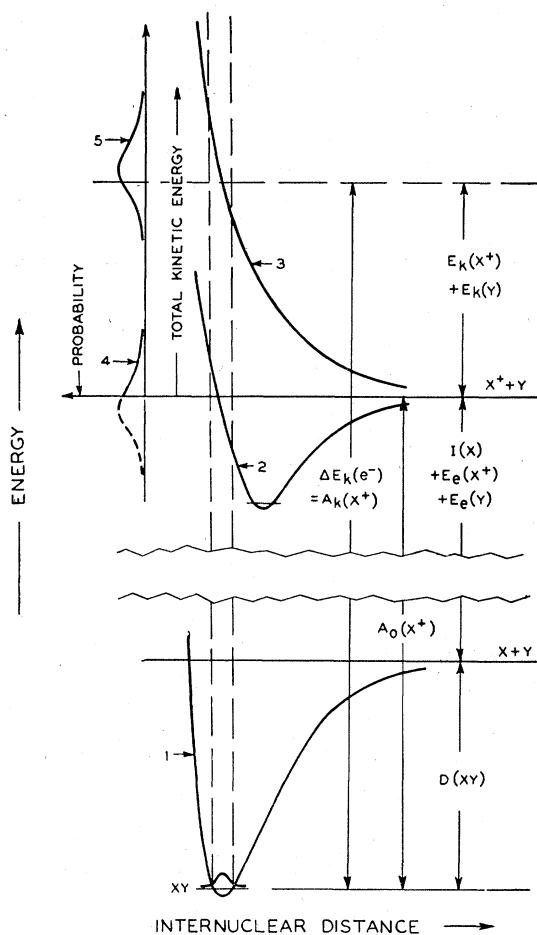


FIG. 1. Typical potential energy curves involved in the dissociative ionization of a diatomic molecule by electron impact. The figure is drawn for a process of type (A) of Table II. Curve 1 is the potential curve of the ground molecular state of XY, curves 2 and 3 of stable and repulsive states of XY⁺, respectively. Curves 4 and 5 are reflections of the square of the ground-state vibrational eigenfunction in the potential curves 2 and 3, respectively. The vertical dashed lines bound the classical Franck-Condon region. The horizontal dashed line represents the final energy level of a transition in which the bombarding electron loses an amount of energy equal to $\Delta E_k(e^-)$. Other symbols are defined in Table I.

¹⁵ This plot has been used extensively by Lozier and Hanson in studies of kinetic energy versus appearance potential without mass analysis (references 1-4).

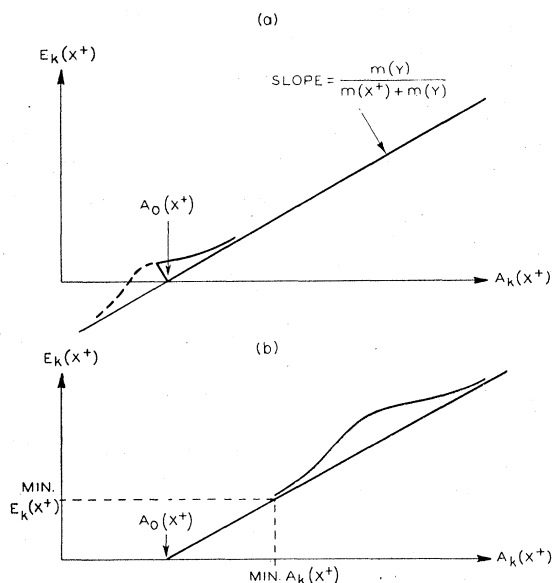


FIG. 2. Plots of ion kinetic energy as a function of appearance potential (called E_k, A_k plots) for dissociative ionization processes described by the potential energy diagram of Fig. 1. Part (a) is drawn for a process represented by transitions to curve 2 of Fig. 1; (b) for transitions to curve 3. The curves 4 and 5 of Fig. 1 representing transition probability as a function of $E_k(X^+)$ are here plotted along the E_k, A_k lines at (a) and (b), respectively, the amplitude normal to the line representing the relative transition probability at the corresponding value of E_k and A_k on the line. Experimental data points may be obtained only over the region in which the ordinate of this probability curve has a value above the minimum set by instrumental detection sensitivity. Symbols used on the figure are defined in Table I.

for more than one dissociative ionization process observed in the same gas, one may generally fix $D(XY)$ unambiguously by comparing the various series. Knowledge of $D(XY)$ then permits fixing of $E_e(X^+) + E_e(Y)$ and, in general, their individual values for each process observed. Examples of this procedure are to be found in Sec. VII of this paper.

Processes of the types (A) and (B) (Table II) may occur for any incident electron energy $E_k(e^-)$ greater than $A_k(X^+)$, the free electrons carrying away after impact the energy by which $E_k(e^-)$ exceeds $A_k(X^+)$. Process (C), on the other hand, being a capture process, demands resonance between the energy of the incident electron and the energy transition induced in the molecule, $A_k(X^+) = E_k(e^-) = \Delta E_k(e^-)$. This results in the interesting properties of these processes discussed in some detail in Sec. IX of this paper.

III. EXPERIMENTAL APPARATUS

The measurements to be described in this paper were made with a mass spectrometer having the special constructional features shown schematically in Fig. 3. Electrons emitted from the filament *A* are accelerated to the desired energy through slits in electrodes *B* and *C* into the ionization chamber bounded by electrodes *C*, *E*, *D*₁, and *D*₂. The beam passes on through the slit in

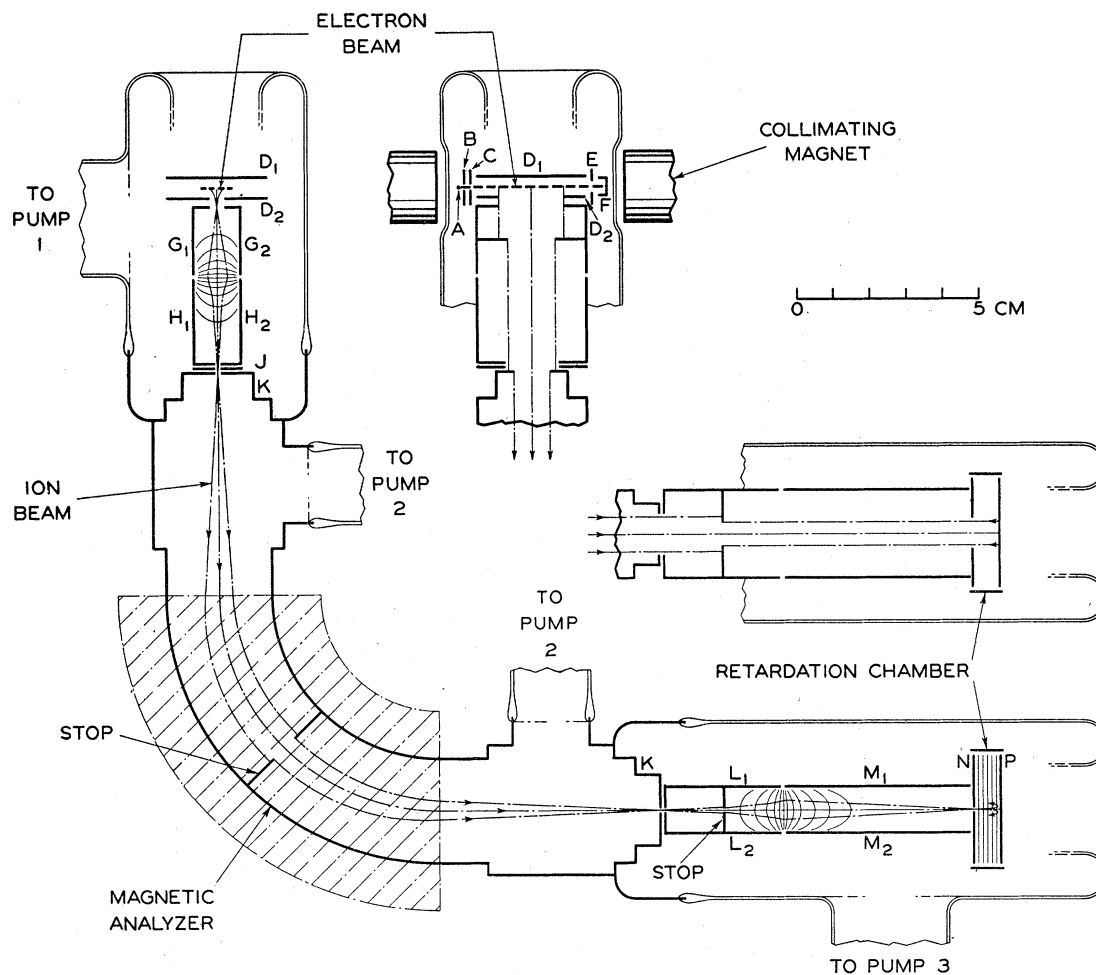


FIG. 3. Schematic view of the mass spectrometer. Views of the electron beam and retardation chamber ends of the apparatus at 90° from the principal view are shown to the right of these portions and above them, respectively. Equipotential lines are indicated in the $G-H$ and $L-M$ ion lenses and in the retardation chamber. Dimensions of the slit in electrode B are $0.08 \text{ cm} \times 1.0 \text{ cm}$; in C , $0.03 \text{ cm} \times 1.0 \text{ cm}$; E , $0.1 \text{ cm} \times 1.2 \text{ cm}$; D_2 , $0.4 \text{ cm} \times 2.0 \text{ cm}$; G_1G_2 , 0.4 cm wide; H_1H_2 , 0.05 cm wide; J , $0.1 \text{ cm} \times 2.0 \text{ cm}$; K (entrance), $0.02 \text{ cm} \times 1.0 \text{ cm}$; K (exit), $0.03 \text{ cm} \times 1.0 \text{ cm}$; L_1L_2 , $0.1 \text{ cm} \times 0.8 \text{ cm}$; N , $0.025 \text{ cm} \times 3.0 \text{ cm}$. Other dimensions may be estimated from the scale of the drawing. The shaded area indicates the extent of the analyzer magnetic field. Typical electrode potentials for $E_k(e^-) = 100 \text{ ev}$ follow: A , -100 volts ; B , -80 v ; C , D_1 , D_2 , and E , zero; F , $+45 \text{ v}$; G_1-G_2 , -15 v ; H_1-H_2 , J , and K , -100 v ; L_1-L_2 , -150 v ; M_1-M_2 and N , -30 v ; P , $-2 \rightarrow +10 \text{ v}$.

E to be collected on F . It is magnetically collimated by a magnet which provides a field strength of 100 oersted at the center of the ionization chamber. Ions formed between D_1 and D_2 are drawn from the ionization chamber by the field fringing from the D_2-G gap. The beam then passes into the $G-H$ lens in which it is focused upon the input slit of the magnetic analyzer K . After m/e analysis the beam is focused by the lens $L-M$ onto the slit in N through which it enters the plane parallel retardation chamber between N and P .

With the instrument one can select any ion formed in the ionization chamber and for it determine the appearance potential for ions having kinetic energies greater than the definite value fixed by the retarding field between electrodes N and P . Further discussion

of the retarding potential and appearance potential measurements is given in the two succeeding sections of this paper.

Ion currents arriving at electrode P are measured with a negative feedback amplifier using a Victoreen 5800 tetrode. Electrode potentials are supplied from specially designed voltage divider circuits operated on dry batteries. The experimental tube is evacuated by three independent two-stage mercury pumps permitting differential pumping on the ionization chamber, analyzer, and retardation chamber sections. Liquid nitrogen traps were used with each of these pumps.¹⁶

¹⁶ The experimental apparatus will be discussed in further detail in a paper on the instrumentation for studies of electron ejection from metals by ion impact to be submitted to the *Review of Scientific Instruments*.

The gases H₂, N₂, and O₂ used in this work were purchased in one liter glass flasks from the Air Reduction Sales Company, Jersey City, New Jersey. The CO and NO used were transferred to 1-liter glass flasks from lecture-size tanks purchased from the Matheson Company, East Rutherford, New Jersey. The CO was passed through a liquid nitrogen trap in the transfer process. The NO was frozen, sublimated, and passed through a dry ice and acetone trap when transferred. The gas was admitted to the ionization chamber through the trap associated with the pump for this chamber. In the study of NO this one trap was cooled with dry ice and acetone. For each gas a study of impurities was made with the mass spectrometer, and in each case it was found that "impurity ions" of the same m/e as those of interest to the experiment were of negligible abundance. The background pressure in the instrument before admission of the gas was always less than 1×10^{-7} mm Hg.

A tungsten filament (A in Fig. 3) was used in the study of CO, N₂, and H₂. For NO and O₂ a so-called combined oxide filament on a platinum nickel base was used. This filament is constructed by drag coating the 95 percent Pt, 5 percent Ni base 6 times with the BaCO₃-SrCO₃ mixture, flashing the filament to 1100°C for 7 seconds between coats. It performed essentially as well in O₂ as in NO, permitting the observation of detail in the appearance potential data missed in earlier work (Sec. V).

IV. RETARDING POTENTIAL MEASUREMENTS

In this section of the paper are discussed the measurements by which ion kinetic energies are determined.

Ions Formed at Rest

Ions from *simple* or *direct ionization*, in which process the atom or molecule loses one or more electrons only, possess essentially the thermal velocities characteristic of the parent gas and may for our purposes be considered to be formed at rest. Retarding potential measurements for such ions enable one to fix the zero point on the kinetic energy [V_P] scale and to evaluate some of the effects of instrumental characteristics on the measurement of kinetic energy distributions.

The retarding potential measurement is made by determining the dependence of current to the electrode P , I_P , as a function of the applied retarding potential V_{NP} . Such retarding potential curves for the Ne⁺ and Ne⁺⁺ ions from the neon calibrating gas are shown in the graphs at the top of Fig. 4. Here, the curves are plotted against V_P , which is taken to be zero at the point of maximum dI_P/dV_P . The derivative dI_P/dV_P is plotted below in each case.

The negative current at values of V_P for which ions can no longer reach P indicates the presence in the retardation chamber of secondary currents due to electrons released at the electrodes by the positive ions. Because of these secondary currents, I_P cannot be

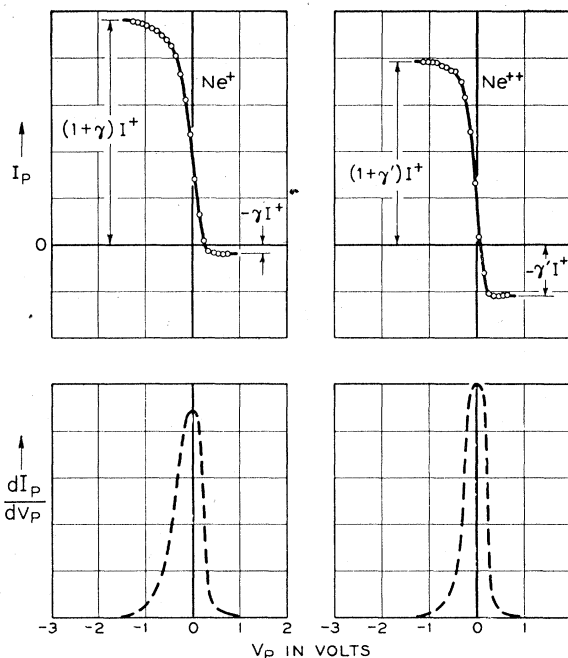


Fig. 4. Retarding potential curves (top) and their derivatives (bottom) for Ne⁺ and Ne⁺⁺ representing ions formed essentially at rest. Current of positively charged carriers to P plotted as positive values above zero axis. Symbols are defined in Table I.

taken directly as a measure of the number of ions arriving at P . Thus, it is necessary to investigate the relation of the measured current $I_P(V_P)$ to the fraction of ions entering the retardation chamber which strike P , $f_P(V_P)$. It will be assumed in this discussion that γ (see Table I) is the same for electrodes N and P and is independent of $E_k(X^+)$, that the numbers of ions reflected as ions or metastable atoms are negligible, that an electron ejected at one electrode can reach the other, and that I^+ is constant. More detailed studies of electron ejection by positive ion impact show these assumptions to be very nearly justified.

For V_P sufficiently negative, $f_P=1$ and $I_P=(1+\gamma)I^+$, I_P thus being made up of the incoming ion current I^+ and the outgoing electron current γI^+ . For V_P sufficiently positive, one has $f_P=0$ and $I_P=-\gamma I^+$, I_P then comprising only the electron current ejected at electrode N . Between these extremes $I_P=(1+\gamma)f_P I^+ - \gamma(1-f_P)I^+$. Here the first term is the incoming ion current and outgoing electron current at P , the second term, the electronic current reaching P from N ejected by the ion current $(1-f_P)I^+$ there. From this expression f_P is seen to be

$$f_P = (I_P + \gamma I^+) / I^+ (1 + 2\gamma).$$

Thus, $f_P(V_P)$ has the same form as $I_P(V_P)$, being obtained from I_P by adding the constant γI^+ and multiplying by the constant $1/I^+(1+2\gamma)$. For this reason retarding potential curves shown in this paper (except Fig. 4) have been shifted so as to be asymptotic to the

V_P axis and are normalized to a convenient ordinate scale. It is interesting to note that it is the current $-\gamma(1-f_P)I^+$ (f_P equal to or near zero) which forms the so-called inverted mass spectrum observed by Fox and Hipple.⁹

The form of the retarding potential curve (Fig. 4) is determined by the inhomogeneity in kinetic energy and the angular spread of the ion beam in the retardation chamber. The latter is of importance because for retardation in a chamber of plane parallel geometry the component of velocity along the field gradient only is decisive. It is difficult to account in detail for the observed distribution in kinetic energy among ions formed at rest, as it depends largely on potential gradients governed by space charge in the region of the electron beam. Evidence to support this statement is to be found in the remarkable insensitivity of the form of the curve to the magnitude of the applied field gradient in the ion source. The form of the dI_P/dV_P curves of Fig. 4 is taken as a calibration of the spread along the retarding potential axis which the instrument introduces for ions formed with any specific initial kinetic energy in the ionization chamber. Despite this total spread of approximately 2 volts for ions of a given initial energy, it is possible to differentiate between ions separated in energy by perhaps 1/10 this amount or less. Thus, for example, in measuring the appearance potential of the ions collected at $V_P=3$ volts, ions of 3-ev kinetic energy will make the largest contribution to the current at onset, despite the fact that some ions of as much as 1 ev less energy will be collected.

The mean position of the retarding potential curve on the V_{NP} scale is determined by contact potential and the factors which determine the ion trajectory in the ionization chamber. The procedure of taking the position of the maximum of the dI_P/dV_P curve for an ion

formed at rest to define the zero point on the kinetic energy scale corrects for contact potential. This calibration method has been demonstrated to be satisfactory by careful investigation of the effect of several factors. By comparison of retarding potential curves at constant $E_k(e^-)$ for the ions $Ne^{++}(m/e=11)$, $CO^{++}(m/e=14)$, $NO^{++}(m/e=15)$, $Ne^+(m/e=22)$, CO^+ and $N_2^+(m/e=28)$, $NO^+(m/e=30)$, and $O_2^+(m/e=32)$, it was demonstrated that the position of the maximum of the dV_P/dI_P curve varies with m/e by less than 0.2 ev over the range studied. This range of m/e includes the values for all ions from dissociative ionization in the gases studied. Variation of electric and magnetic fields in the ion source over ranges greater than normally used also produced no greater than a 0.2-volt shift. The retarding potential curve was found to shift by two to three times this amount, however, when the bombarding electron energy was varied over the range from 30 to 100 ev.

In the measurement of both onset potential and kinetic energy, since $E_k(e^-)$ is then varied, care must be taken to calibrate the kinetic energy scale in the $E_k(e^-)$ region where measurements are made. This latter procedure cannot be followed for the O^- ions formed by the resonance capture process [(C) of Table II] for which the kinetic energy scale must be calibrated against O^- ions from another ionization process at higher $E_k(e^-)$ [(B) of Table II]. The details of the procedure followed in this instance and an independent check upon its accuracy are discussed in Sec. IX. The effect of variation of electron beam current was not studied, although it could conceivably have an effect by virtue of electronic space charge (compare its possible effect on appearance potential measurements, Sec. V). The electron beam current was held constant during retarding potential measurements and calibration of the kinetic energy scale.

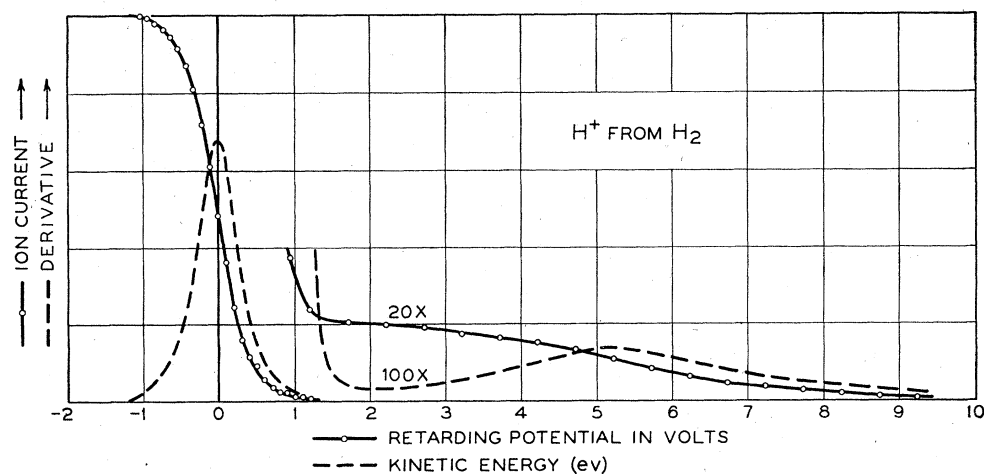


FIG. 5. Retarding potential curve and its derivative for H^+ ions from dissociative ionization of H_2 . $E_k(e^-) = 100$ ev. The curve has been normalized to a convenient ordinate scale. Ions near zero kinetic energy are from the $1s\sigma^2\Sigma_g^+$ state; ions possessing appreciable kinetic energies are from the repulsive $2p\sigma^2\Sigma_u^+$ state of H_2 .

Ions Formed with Kinetic Energy

Ions formed from dissociative ionization have initial kinetic energies distributed over quite wide ranges (curves 4 and 5 of Fig. 1). It is the task of the kinetic energy measurement for these ions to determine the nature of the kinetic energy distribution from the retarding potential curves.

The derivative of the retarding potential curve is expected to deviate from the true distribution in initial kinetic energy by virtue of three effects of instrumental origin. These are (1) the spread along the retarding potential scale of ions having a specific kinetic energy, (2) the discrimination at the slits in the source and analyzer of the mass spectrometer against collection of ions having appreciable initial energies, and (3) the velocity dispersion of the analyzer.

The first of these effects has been evaluated for the present instrument in the measurement of retarding curves for ions formed at rest. The second effect results from the discrimination against final collection of ions having appreciable components of velocity normal to the course of the beam through the instrument. Because ions which start with very low velocities are more easily formed into a beam than those with appreciable initial velocities randomly directed, they are collected with greater over-all efficiency.^{6,7,17} The third effect arises from the dependence upon initial energy of the settings of the ion accelerating potential and analyzer magnetic field strength for passage of the ion through the exit slit. If ions of zero energy are formed, it has been usual to set the analyzer to collect these ions and to maintain this adjustment throughout the retarding potential measurement. Then the velocity dispersion further discriminates against collection of ions of greater initial energy. The effect of velocity dispersion is nicely illustrated in measurements made on O⁻ from NO shown in Figs. 16 and 17 and discussed in Sec. IX of this paper. Quantitative evaluation of these discriminatory effects is not practicable.

A test of the retarding potential measurement has been made by studying H⁺ from H₂, for which the potential curves involved are known and upon which considerable previous experimental work has been done. In Fig. 5 are shown the measured retarding potential curve and its derivative. It is clear that the derivative curve is compounded of two curves like curves 4 and 5 of Fig. 1 modified by the instrumental discrimination in favor of collection of ions of zero initial energy. These results are in excellent agreement with the results of Bleakney⁵ and Lozier¹ as well as the measurement of ion peak shape for H⁺ ions by Hagstrum and Tate (their Fig. 10).^{6,18}

¹⁷ N. D. Coggeshall, J. Chem. Phys. 12, 19 (1944).

¹⁸ H. F. Newhall [Phys. Rev. 62, 11 (1942)] did not observe the H⁺ ions of zero initial energy. This failure must be of instrumental origin and may well be the result of velocity dispersion in the analyzer. Were, as seems likely, the accelerating potential and magnetic field adjusted to optimum collection of the ions with

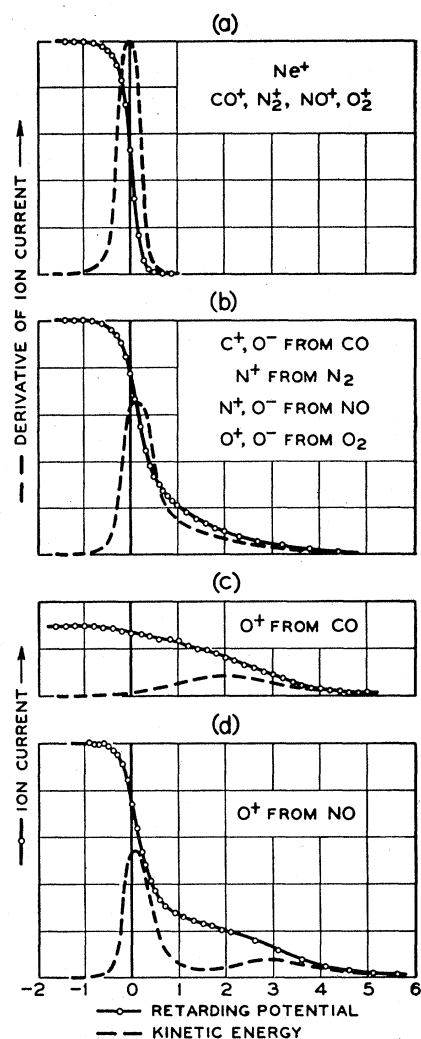


Fig. 6. Retarding potential and derivative curves for ions formed at rest [part (a) of the figure]; and of three distinguishable types [parts (b), (c), and (d)] for ions from dissociative ionization by electron impact in the gases CO, N₂, NO, and O₂. The curves were taken at $E_k(e^-) = 100$ ev and have been normalized to convenient ordinate scales which bear no meaningful relation to one another. In parts (a) and (b) the experimental curves are for the first ion listed.

In Fig. 6 are shown retarding potential curves and their derivatives for the different types of distribution in initial energy observed for ions in CO, N₂, NO, and O₂ and the calibrating gas Ne. In part (a) of the figure is reproduced the Ne⁺ curve for ions having zero initial energy only. Curves for the molecular ions, CO⁺, N₂⁺, NO⁺, and O₂⁺ are essentially indistinguishable from the Ne⁺ curve. The curves of parts (b), (c), and (d) are for ions from dissociation processes. In the first of these,

high kinetic energy, a readjustment would be necessary to observe the ions of zero energy in any quantity. In fact, an estimate of the velocity dispersion of Newhall's instrument shows it to be sufficient essentially to exclude completely the ions of zero energy when adjusted for optimum collection of the most abundant H⁺ ions having high initial energies (5 ev).

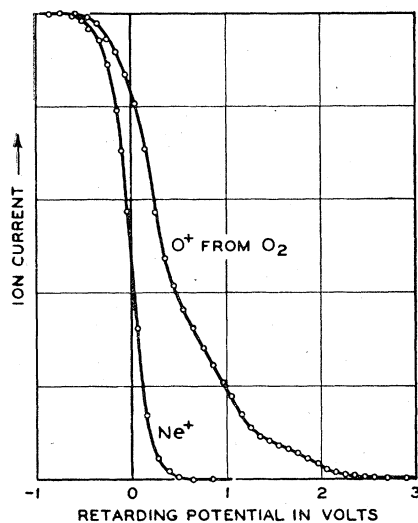


FIG. 7. Retarding potential curve for O^+ from O_2 showing structure indicative of distinguishable groups of ions having different kinetic energies. The curve for Ne^+ is included for comparison and to calibrate the retarding potential scale. $E_k(e^-) = 45$ ev, thus below $A(O_2^{++})$.

(b), ions of zero initial energy are present, the upper potential curve involved and kinetic energy distribution being like curves 2 and 4 of Fig. 1, respectively. The curves at (c) for O^+ ions from CO indicate that all the O^+ ions possess appreciable initial energies, the process of their formation thus involving a potential curve and yielding a distribution function like 3 and 5 of Fig. 1, respectively. Since the instrumental discriminations vary slowly for ions all having appreciable energies, the derivative curve of Fig. 6(c) approximates quite closely the distribution curve 5 of Fig. 1. O^+ ions from NO

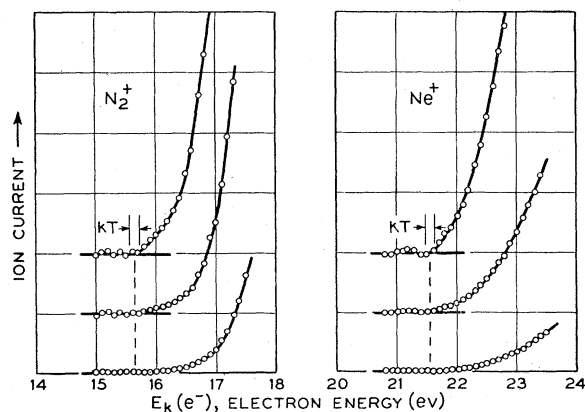


FIG. 8. Appearance potential data for the ions N_2^+ from N_2 and Ne^+ from Ne plotted in the top curves to an ordinate scale of sufficient extension to show the break at the onset of the ionization process as well as the random fluctuations of the data points. Below these curves the same data are plotted to ordinate scales reduced in extension for each curve by a factor 4 over that of the curve above. Note the disappearance of the break in these latter curves. The energy interval kT corresponding to the electron beam filament temperature is indicated. The scale of $E_k(e^-)$ has been calibrated by taking $A(Ne^+) = I(Ne) = 21.56$ volts.

gave the retarding potential curve at (d) in Fig. 6. It appears to be a superposition of curves like those at (b) and (c) and thus to resemble the curve obtained for H^+ from H_2 (Fig. 5). The dissociative ionization processes responsible for these ions are discussed in detail in Sec. VIII.

The derivative curves of Fig. 6 are recognized to reproduce the four types of ion peak shapes observed by Hagstrum and Tate⁶ for the same ions in these gases. This agreement confirms the essential correctness of both methods of determining initial energy. The present results also agree well with most of Berry's⁷ determinations of kinetic energy. Evidence of groupings of ions which Berry finds in the kinetic energy distributions for a number of ions is found in this work only for O^+ ions from O_2 , however. Although its general classification is that of Fig. 6(b), the O^+ retarding potential curve (Fig. 7) does show structure corresponding in a general way to that observed by Berry. The present work is in disagreement with Berry's conclusion that all O^+ ions from NO have at least 2-ev kinetic energy.

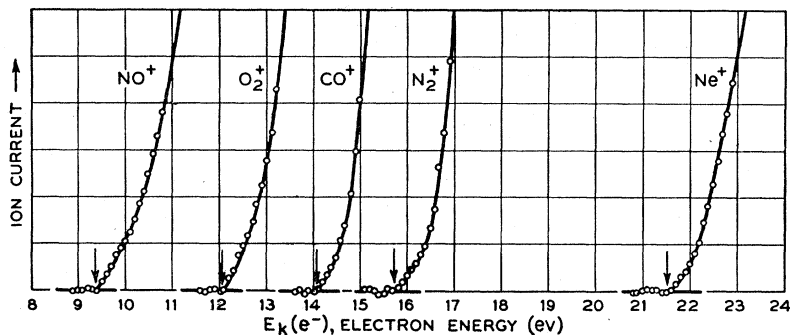
V. APPEARANCE POTENTIAL MEASUREMENTS

As is well known, the measurement of appearance potential of an ion consists in determining the minimum electron energy required to form the ion. *Contact potential* is determined by repeating the process for a noble gas ion (in this work Ne^+), whose appearance potential is known to be the ionization potential of the atom (Fig. 8). Any dependence on the *form of the ionization probability function* is presumably eliminated by identifying the appearance potential with the initial break in the ion current curve. The effect of the *thermal velocity distribution of the bombarding electrons* is to add an exponential tail to the ion current curve below the onset potential¹⁹ and is thus to eliminate any initial break when it is looked for to a scale fine relative to kT . The position of the breaks observed in the data reported here are considered uncertain to at least $kT = 0.15$ ev, and no greater accuracy than ± 0.2 ev is claimed. The effect of *instrumental detection sensitivity* on the ability to locate the appearance potential is illustrated in Fig. 8. The over-all detection sensitivity depends, to be sure, not only on the sensitivity of the ion current detector but also on the magnitude of the electron beam current and gas pressure which can be maintained in the ionization chamber.

Appearance potential data obtained in this work are plotted in Figs. 9, 10, 11, 14, 15, and 18. These data are in excellent agreement with previous work (Secs. VI-IX), with the exception of the data for O^+ and O^- in O_2 . In the only other recent work on the dissociative ionization processes of types (A) and (B) in oxygen, Hagstrum and Tate⁶ missed the structure in the data for O^+ and O^- ; and as a result, misplaced on the elec-

¹⁹ See theory of G. H. Wannier reported by R. E. Honig, J. Chem. Phys. 16, 105 (1948).

FIG. 9. Appearance potential data for the molecular ions from NO, O₂, CO, and N₂. The electron energy scale is calibrated against $A(\text{Ne}^+) = I(\text{Ne}) = 21.56$ volts. The indicated unit of the ordinate scale is approximately 0.3 percent of ion current at $E_k(e^-) = 100$ ev in each case. The detection limit is approximately 5 percent of this, or one part in about 6700 of ion current at 100-ev electron energy. The appearance potentials extracted from these data are given in Table III.



tron energy scale the resonance peak for O⁻ ions from the capture process of type (C).²⁰ The study of oxygen was difficult in this earlier work because of the poisoning effect of the gas on the uncombined oxide filament used. In the present work, the use of a combined oxide-coated filament (Sec. III) made the experiment in oxygen no more difficult than that in other gases. There is little doubt that the present results represent the situation in O₂ correctly. The new data will be seen in Sec. VII to bring the electron impact work into excellent agreement with the band spectroscopic data for O₂.

Two other aspects of the measurement of appearance potentials are illustrated in the data for O⁺ and O⁻ from O₂ in Fig. 10. The first is the difficulty of observing the onset of a process when it occurs at higher electron energy than the onset of another relatively more abundant process. The process yielding O⁻ ions at 22.0 ev must also give rise to O⁺ ions. However, at 22.0 ev the O⁺ ion current is rising rapidly by virtue of the ions

from the process yielding O⁺+O which commences at 20.8 ev, and no break is seen. The dashed line below the O⁺ curve above 22.0 ev, drawn below the curve by the amount the similar dashed line lies below the O⁻ curve in this energy range, demonstrates clearly the impossibility of picking out a break of the magnitude to be expected on such a rapidly rising background current. In the second place, close scrutiny of the O⁻ curve shows a small rise in current at about 20.8 ev, where the strong O⁺ onset occurs. This is believed not to be a bona fide appearance of O⁻ ions, which should then appear in amount equal to the O⁺ ions, but the result of O⁺ space charge rearranging the O⁻ ion trajectories in the ion source so as to increase slightly the instrumental collection efficiency. The interpretation of the onset potentials in Sec. VII confirms this view.

A final comment on the measurement of appearance potential concerns the effects of field gradients and space charge in the ionization chamber of the mass spectrom-

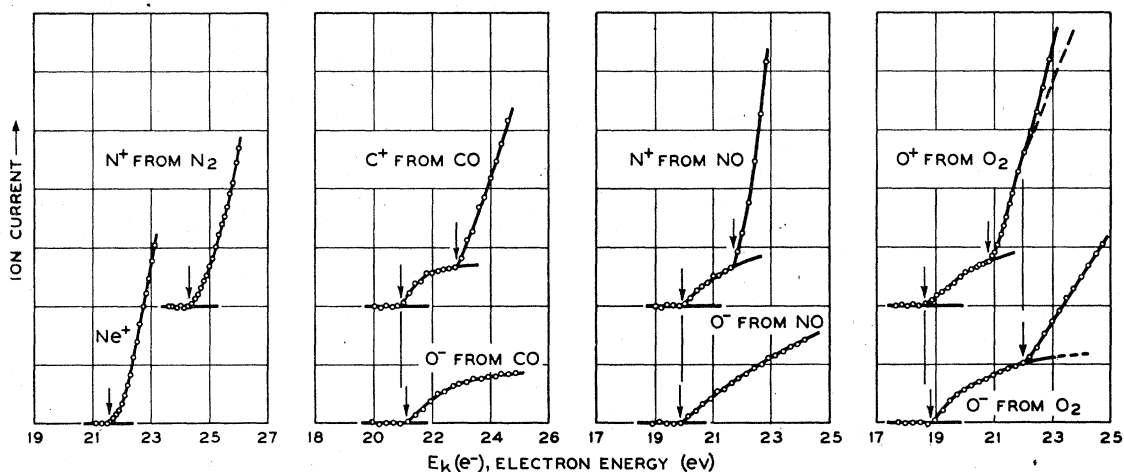


FIG. 10. Appearance potential data for ions of zero initial kinetic energy from dissociative ionization in N₂, CO, NO, and O₂. These are data for ions having retarding potential curves of the type shown at (b) in Fig. 6. The electron energy scale is calibrated against $A(\text{Ne}^+) = I(\text{Ne}) = 21.56$ volts. The indicated unit of the ordinate scale is approximately 1 percent of the ion current at electron energy = 100 ev. The detection limit is approximately 5 percent of this or about one part in 2000 of ion current at $E_k(e^-) = 100$ ev. The appearance potentials extracted from these data are given in Table IV.

²⁰ Inspection of the original data of Hagstrum and Tate shows that in the data of their Fig. 19 only the second break at higher electron energies was observed. Later, when calibrating against a positive ion, the first break was observed, but not enough data taken then to reveal the second. This confusion of the two onsets displaced the resonance peak to lower energies by the difference between them. When properly interpreted, the experimental data agree well with the newer results (Table VII).

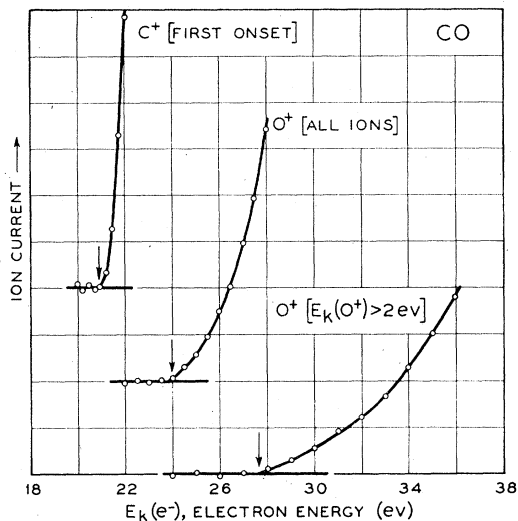


FIG. 11. Appearance potential data for O^+ ions from CO. The appearance potential in each case corresponds to the ion of lowest kinetic energy in the group specified in the brackets alongside each curve. The curves labeled "all ions" and " $E_k(O^+) > 2\text{ eV}$ " correspond to retarding potentials of -2 and $+2$ volts, respectively. The electron energy scale is calibrated against the first appearance potential of C^+ ions from CO at 20.9 eV (see Fig. 10 and Table IV). The indicated unit of the ordinate scale (about 1×10^{-16} amp) is approximately 0.2 percent of the ion current at $E_k(e^-) = 100$ eV. The detection limit is about 10 percent of this, or about one part in 5000 of the ion current at $E_k(e^-) = 100$ eV. The data points plotted are the averages of those obtained in several runs. The appearance potentials extracted from these data are included in Table VII.

eter. In the present case the field in the region where ions are formed is that which fringes from the D_2-G gap (Fig. 3). This field should change the velocity of the bombarding electrons²¹ and thus manifest itself when appearance potentials of positive and negative ions are intercompared. As this requires the reversal of the ion accelerating field, the electron energy scale would be expected to shift by twice the potential difference between the point where ions are formed and the ionization chamber walls. Electrolytic tank measurements with a large scale model of the ion source and first ion slits shows this potential difference to be about 0.9 volt. That such a shift does not occur can be seen from the good agreement between the appearance potentials measured for positive and negative ions from the same process in CO, NO, and O_2 (Fig. 10). It would appear that this can be attributed only to the circumstance that the potential in the electron beam is determined by the space charges within it and not by the small field in which the beam is placed.

A theoretical determination of the beam potential is difficult, but a rough calculation shows that the potential depression due to a 20-volt electron beam of 1 ma amounts to several volts.²² Such a potential depression

²¹ The author is indebted to Dr. J. Blears of Manchester for an illuminating discussion on this point.

²² The author is indebted to his colleague Dr. J. R. Pierce for a helpful discussion of these effects.

will fill in with positive ions until an equilibrium potential is reached which enables ions to escape as rapidly as they are formed. The beam can remain "filled" with ions at electron energies in the ionization chamber below the lowest appearance potential of any positive ion if the electron energy exceeds this value at other points along the beam and the field is such as to bring the ions into the ionization chamber. In the present experiment these conditions are met between electrodes E and F (Fig. 3) and between electrodes B and C. Very weak ion currents at electron energies in the ionization chamber below the lowest appearance potential constitute evidence of ionization at these points. These currents decrease as V_{AB} and V_{EF} are reduced. It is perhaps essential that this ionization be maintained so as to keep space-charge conditions along the beam constant as the electron energy in the ionization chamber is varied.

Despite the indefinite picture one has as to the theory and detail, the experimental situation is plain. Equivalence of the onset potentials mentioned above is confirmed by the work of Lozier³ in CO, in which, by means of an apparatus having a *field free* ion source, C^+ and O^- ions were shown to appear first at the same electron energy (20.9 eV) as in this work. Furthermore, the breadth of the velocity distribution curve for ions formed at rest [Figs. 4 and 6(a)] is quite insensitive to the applied field gradient in the ion source. Finally, the measurement of appearance potentials has been shown to be independent, within experimental error, of the variation of the voltage $V_{G_1G_2}$ over the range necessary to bring ions of different m/e to maximum collection efficiency.

At this point we turn from a discussion of theory and measurement to a detailed examination of the experimental results.

VI. SIMPLE MOLECULAR IONIZATION IN CO, N_2 , NO, AND O_2

The appearance potential data for the molecular ions in the gases studied are shown in Fig. 9. In Table III these values are compared with other electron impact values. The electron impact methods agree well

TABLE III. Appearance potentials of molecular ions.

Ion	Appearance potential		Ionization potential from other sources ^b
	Present work	Previous work ^a	
CO^+	14.1 ± 0.2	14.1, ^c 14.1, ^d 13.9 ^e	14.00 ₉
N_2^+	15.7 ± 0.2	15.7, ^e 15.65, ^f 15.7, ^d 15.8 ^e	15.576
NO ⁺	9.4 ± 0.2	9.5, ^e 9.5, ^f 9.5 ^d	...
O_2^+	12.1 ± 0.2	12.3, ^e 12.5 ^d	12.2

^a Only those electron impact values obtained with instruments having a transverse, magnetically collimated electron beam are included.

^b As given by G. Herzberg, *Spectra of Diatomic Molecules*, reference 12, Table 37, p. 459.

^c Reference 6.

^d J. T. Tate and P. T. Smith, *Phys. Rev.* **39**, 270 (1932).

^e A. L. Vaughan, *Phys. Rev.* **38**, 1687 (1931).

^f Tate, Smith, and Vaughan, *Phys. Rev.* **48**, 525 (1935).

on a unique value for each potential, which, in turn, agrees well with the molecular ionization potential from other sources. One should expect the "vertical" ionization potential which the electron impact method measures to agree with the "adiabatic" ionization potential only if the probability distributions in internuclear distance in the ground states of the molecule and molecular ion overlap. This is known²³ to be the case for CO, N₂, and O₂. No data on the ground state of NO⁺ are available.

VII. DISSOCIATIVE IONIZATION IN CO, N₂, NO, AND O₂

The dissociative ionization processes in CO, N₂, NO, and O₂ have been identified by the procedures outlined in Sec. II using the onset potential data listed in Table IV. The processes observed are listed in Table V. For processes of types (A) and (B) the appearance potentials listed in Table IV were obtained from the data plotted in Fig. 10. For each of these processes it has

TABLE IV. Appearance potentials, A_0 , of ions from dissociative ionization.^a

Molecule	Ion	Appearance potential (A_0)	
		Present work	Previous work ^b
CO	C ⁺	20.9±0.2	20.9 ^e , 20.9 ^f
		22.8±0.2	22.8 ^e , 22.8 ^f
	O ⁺	23.2±0.3	23.3 ^e
	O ⁻	9.6±0.2 21.1±0.2	9.5, ^e 9.5, ^f 9.5, ^g 9.3 ^h 20.9, ^e 20.9 ⁱ
N ₂	N ⁺	24.3±0.2	24.3, ^e 24.27, ⁱ 24.5 ^g
		NO	N ⁺
21.7±0.2	21.8, ^e 21.7, ⁱ 22 ⁱ		
(18.9) ^e	...		
(21.3) ^e	...		
NO	O ⁺	...	3.2 ^j
		5.3±0.4	...
	O ⁻	19.8±0.2	20.0 ^e
	O ₂	O ⁺	18.6±0.2
20.8±0.2			...
(22.0) ^d		...	
O ⁻		2.9±0.4	2.9 ^f
...	12.0 ^f		
18.8±0.2	18.9, ^e 18.9 ^f		
22.0±0.2	...		

^a Note that these are the appearance potentials for ions of zero initial energy. The kinetic energy of these ions has been measured and $A_0(X^+)$ determined by the methods described in the text.

^b Only those electron impact values are included which have been obtained with instruments having a transverse, magnetically collimated electron beam. Vaughan's (reference g below) single value of 22.5 volts for $A(C^+)CO$ and Hagstrum and Tate's (reference 6) single value of 19.2 volts for $A(O^+)O_2$ are excluded because both of the close-lying onset potentials were not observed, and the potential given may represent some sort of average value.

^c This value cannot be said to have been measured in this work, but the evidence is that ions are formed from a process having this as its dissociation limit (see detailed discussion in Sec. VIII).

^d For reasons given in Sec. V this value cannot be said to have been measured in this work, but the onset of O⁺ ions at this value is inferred from the appearance of O⁻ there (see text in Sec. VII).

^e Reference 6.

^f Reference 3.

^g Reference e of Table III.

^h Reference 4.

ⁱ Reference 2.

^j Reference 4.

²³ The values of r_e for the ground states XY and XY⁺ in these molecules are given by G. Herzberg, reference 12, Table 39. The widths of the vibrational eigenfunction in the ground states may be obtained from Fig. 42, p. 77, and accompanying text.

TABLE V. Dissociative ionization processes observed in CO, N₂, NO, and O₂.

Process	Energy level of dissociation limit (A_0)	
	Experimental ^a	Calculated ^b
(A) CO($X^1\Sigma^+$) → C ⁺ ($^2P^0$) + O [*] (1D)	22.8	22.84
(B) → C ⁺ ($^2P^0$) + O [*] (2.2)	20.9	20.87
(A') → C(3P) + O ⁺ ($^4S^0$)	23.2	23.22
(C) → C(3P) + O [*] (2.2)	9.5	9.61
(A) N ₂ ($X^1\Sigma_g^+$) → N ⁺ (2P) + N [*] ($^2D^0$)	24.3	24.30
(A) NO($X^2\Pi$) → N ⁺ (2P) + O [*] (1D)	21.7	21.81
[N ⁺ (1D) + O(3P)] ^c		[21.74]
(B) → N ⁺ (3P) + O [*] (2.2)	19.9	19.84
(A') → N($^4S^0$) + O ⁺ ($^4S^0$)	...	18.91
(A') → N [*] ($^2D^0$) + O ⁺ ($^4S^0$)	...	21.30
(C) → N($^4S^0$) + O ⁻ ($^2P^0$)	3.2	3.1
(C) → N($^4S^0$) + O [*] (2.2)	5.3	5.3
[N [*] ($^2D^0$) + O ⁻ ($^2P^0$)] ^c		[5.5]
(A) O ₂ ($X^3\Sigma_g^-$) → O ⁺ ($^4S^0$) + O [*] (1D)	20.8	20.66
(B) → O ⁺ ($^4S^0$) + O [*] (2.2)	18.7	18.69
(B) → O ⁺ ($^2D^0$) + O [*] (2.2)	22.0	22.01
(C) → O(3P) + O ⁻ ($^2P^0$)	2.9	2.88
(C) → O [*] ($^5S^0$) + O ⁻ ($^2P^0$)	12.0	12.02

^a These values represent the averages of slightly variable experimental values given in Table IV.

^b Calculated using the dissociation energies given in bold-faced type in Table VI.

^c A second possibility for this process which cannot be excluded.

^d This onset potential cannot be said to have been determined in this work although there is good evidence that the process occurs (see Sec. VIII).

been demonstrated that ions of zero initial kinetic energy are formed, the retarding potential curves being of the type shown at (b) in Fig. 6. The positive ions C⁺, N⁺, and O⁺ from CO, NO, and O₂, respectively, undoubtedly come primarily from processes of type (A). That these ions are formed with zero energy in the processes of type (B) is demonstrated by the fact that retarding potential measurements show O⁻ ions of zero energy. Thus, the onset potential for a process of type (A) or (B) in these gases, measured when ions of all initial energies are collected, gives directly the energy level of the dissociation limit of the process above the ground state of the molecule. For the other processes observed, A_0 is determined from the appearance potential and retarding potential measurements as discussed in Secs. VIII and IX. In this paper A_0 values (Table IV) are separated from A_e values (Table VII).

The excellent agreement among the results of this and earlier work listed in Table IV would appear to make possible now a definitive statement concerning the nature of the processes and the energies involved in their onset potentials. Certainly, this is true for CO, NO, and N₂. Despite the shortcomings of previous work in O₂, it is believed that a similar position is justified with respect to the present results for this molecule also. From the experimental values of A_0 summarized in Table V, a series of values of the dissociation energy of the molecule involved has been calculated assuming all possible excitations of the products. These are listed in Table VI. It is evident that for CO, NO, O₂, and, as will be seen, for N₂ also, only a single value of $D(XY)$

TABLE VI. Dissociation energies calculated from A_0 for various choices of excitation energies.

Molecule	Process (Table II)			
	(A)	(B)	(A')	(C)
CO				11.7
	11.6	11.8		10.4
	9.6	9.6	9.6	9.5
	7.4	6.5	8.3	9.0
	6.4	4.3	6.9	8.2
		6.3		
N ₂	9.8			
	7.9			
	7.4			
	6.2			
	5.7			
NO		7.6		
	7.2	5.7		7.5
	5.3	5.4		5.3
	5.2	3.5		3.1
	3.3			2.9
	3.2			1.1
O ₂				14.2 ^b
		10.6		12.2
		8.4		12.0
		7.3		10.0
	7.2	7.3	5.6	7.8
	5.2	5.1	5.1	5.1
	3.9	4.0	3.4	3.1
	3.0	1.8		2.9
				0.9

^a These values are calculated from Hanson's datum (reference 4), $A_0(O^-)NO = 3.2$ v, for a process not observed in this work (see Sec. IX of text).

^b These values are calculated from Lozier's datum (reference 3), $A_0(O^-)O_2 = 12.0$ v for a process not observed in this work (see Sec. IX of text).

(shown in bold-faced type in Table VI) can satisfy the demands of the appearance potential data. These agree well with the spectroscopic values given by Hagstrum¹⁰ for $D(CO)$ (9.605 eV) and by Herzberg²⁴ for $D(N_2)$ (7.373 eV) and $D(NO)$ (5.296 eV). Further discussion of $D(CO)$, $D(N_2)$, and $D(NO)$ for which no one value is now universally accepted is given in Secs. X and XI. A unique value of $D(O_2)$ in excellent agreement with the accepted value of 5.080 eV is now obtained.

The value of $EA(O) = 2.2$ eV (Sec. XII) is used in the calculations of $D(XY)$ from data for processes (B) and (C) in CO and NO. The excitation of O^- assumed in these calculations is the only one considered possible on theoretical grounds, namely, $E_e(O^-) \cong EA(O) = 2.2$ eV (Sec. XIII). This state has been designated $O^{*-}(2.2)$ in this work. In N_2 the electron impact data alone cannot fix $D(N_2)$, but the 7.4-eV value is the only one compatible with the data for NO, as will be discussed in Sec. XI.

Thus, the electron impact data specify a unique assignment of dissociative ionization processes in CO, N_2 , NO, and O_2 . In Table V are indicated the states of excitation of the products and the experimental and calculated values of the energy level above the ground molecular state of the dissociation limit of each process.

²⁴ G. Herzberg, reference 12, p. 448 ff. and Table 39.

VIII. PROCESSES YIELDING O^+ IN CO AND NO

It is evident that the O^+ ions observed in CO and NO require special attention. Hagstrum and Tate⁶ demonstrated, for example, that all the O^+ ions from CO possess initial kinetic energy and the recognition of this fact leads to a satisfactory interpretation of the process of their formation. These results are confirmed in detail by the present work. The retarding potential curve yields a velocity distribution [Fig. 6(c)] which is in excellent agreement with the peak shape of Hagstrum and Tate (their Fig. 8). Thus, the process responsible for these ions is one which involves an upper potential curve like that at 3 in Fig. 1 yielding a distribution of initial energies like curve 5 in Fig. 1. The discrimination of the mass spectrometer against collection of ions having appreciable initial velocities accounts for the low resolved currents measured for this ion [25 percent of the $C^+(CO)$ ion current].

The measurement of appearance potential for an ion such as this without heed to the initial kinetic energy involved will yield a result which depends upon the characteristics of the mass spectrometer and on the procedure followed. If the mass spectrometer has high velocity dispersion in the analyzer, so that ions of only a small range of kinetic energies can pass through at given ion accelerating voltage and magnetic field, and if one adjusts to the maximum of the peak, the appearance potential will be that of ions at the maximum of the velocity distribution [maximum of the derivative curve at (c) in Fig. 6]. This is the nature of Tate, Smith, and Vaughan's measurement of 27 volts (Table VII), checked by Hagstrum and Tate for the maximum of the ion peak. If, on the other hand, the spectrometer has lower velocity dispersion, so that some ions of every initial velocity can be collected simultaneously, the appearance potential measurement will yield a result characteristic of the lowest initial energy in the dis-

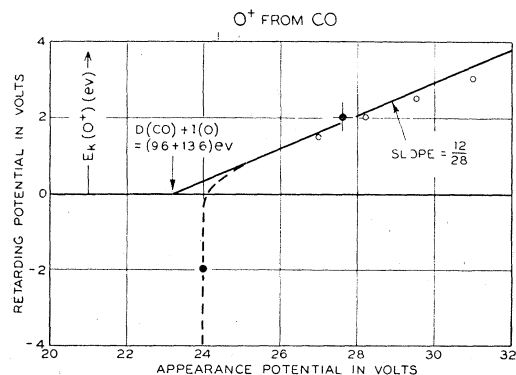


FIG. 12. Plot of retarding potential vs appearance potential for O^+ ions from CO. Filled circles at +2 and -2 volts retarding potential show data from this work. Open circles represent data of Hagstrum and Tate (reference 6), for which the retarding potential scale is replaced by the equivalent scale of displacement across the peak on the ion accelerating voltage scale. The line of slope 12/28 is drawn through the point [$A_k(O^+) = D(CO) - I(O) = 23.2$ v; $E_k(O^+) = 0$] in the E_k, A_k portion of the graph.

tribution. This is the nature of the measurement made in this work when the potential V_P was set such that all ions were collected (Fig. 11).

The determination of the dissociation limit for the process yielding O⁺ from CO must involve the simultaneous measurement of appearance potential and initial kinetic energy and the determination of the E_k , A_k line shown in Fig. 2(b). In the present work the measurement of appearance potentials for O⁺ ions in CO was found very difficult because of the strong instrumental discrimination against collection of these ions. The appearance potentials obtained from the data of Fig. 11 are plotted in Fig. 12 together with some data of Hagstrum and Tate.⁶ Clearly, the data agree very well, considering the difficulty of the measurements, and lie within experimental error on the line of proper slope through the value $A_0(\text{O}^+)_{\text{CO}} = 23.2$ ev. This determination of A_0 is not to be considered as an extrapolation of the E_k , A_k data, it must be emphasized, because the slope of the line on which they should lie is known. More properly, the determination is a calculation of an average value of A_0 from the E_k , A_k measurements by the relation between these quantities dictated by the conservation of momentum on dissociation. The value $A_0 = 23.2 \pm 0.3$ ev is thus listed in Table IV as a dissociation limit and the A_k values listed in Table VII. The process yields unexcited products (Table V).

The study of the O⁺ ion from CO has been discussed in some detail not only because of the interest which attaches to it by virtue of the special nature of the process involved, but also because of its importance with respect to the dissociation energy of carbon monoxide and the sublimation energy of carbon (Sec. X).

For O⁺ ions from NO the velocity distribution shown at (d) in Fig. 6 was obtained in this work. Except for differences in relative heights of the two peaks, the form is seen to agree well with that determined from the ion peak shape by Hagstrum and Tate⁶ (their Fig. 17). It now seems clear that there are in all probability *two* processes of formation of the O⁺ ions from

TABLE VII. Appearance potentials, A_k , of ions possessing initial kinetic energy, E_k .

Process	Present work	A_k Previous work	E_k
CO → C(³ P) + O ⁺ (⁴ S ⁰)	24.0	27 ^{a, b}	0.3 (minimum) 1.5 (for most abundant ion)
NO → N(⁴ S ⁰) + O ⁺ (⁴ S ⁰)	20.6	20.5, ^b 21 ^c	0.8 (minimum)
→ N(⁴ S ⁰) + O ⁺ (² D ⁰)	7.4	7.0, ^b 6.8 ^c	0.9 (minimum)
O ₂ → O(³ P) + O ⁻ (² P ⁰)	6.3	6.1, ^d 6 ^c	1.7 (minimum)

^a Reference f of Table III.

^b Reference 6.

^c Reference d of Table III.

^d The value of 3.0 volts given by Hagstrum and Tate (reference 6) is in error. This corrected value is obtained by subtracting the 15.9-volt difference between the two O⁺ onsets observed by Hagstrum and Tate from the third onset (22.0 volts) observed in the present work (see reference 20).

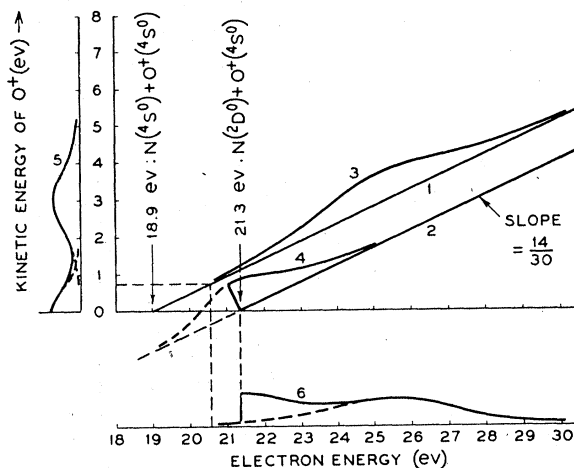


FIG. 13. Suggested E_k , A_k plot for dissociative ionization processes yielding O⁺ ions from NO. Lines 1 and 2 are the E_k , A_k lines for the processes identified at their respective A_k asymptotes (A_0). Curves 3 and 4 are the suggested transition probabilities drawn in the manner of Fig. 2. Curve 5 is the projected sum of curves 3 and 4 onto the E_k axis; curve 6, the projected sum of curves 3 and 4 onto the A_k axis. Curve 5 represents the distribution of ion kinetic energies; curve 6, the relative probability of formation of an ion having a specified A_k . The vertical dashed lines indicate the minimum appearance potentials, the horizontal dashed line and the A_k axis ($E_k = 0$), the minimum kinetic energies of O⁺ ions from the two processes. The figure is constructed so as to place the minimum appearance potential for the process NO → N(⁴S⁰) + O⁺(⁴S⁰) at the observed appearance potential of 20.6 volts.

NO and that an explanation of the observed facts should be given on this basis. The two observations now in hand, (1) that ions of zero energy are formed and (2) that the appearance potential, if assumed to be that of ions of zero energy, does not fit the energy scheme based on the measurements for other ions (Tables V and VI), lead one to this conclusion. In one process ions of zero initial energy are formed; in the other they are not. Thus, the situation is much like that which obtains for H⁺ ions from H₂ [compare Figs. 5 and 6(d)]. The successful explanation of the appearance potential measurement makes it necessary, however, to assume different dissociation limits for the two processes yielding O⁺ in NO. Figure 13 shows the proposed interpretation in terms of E_k , A_k plots for the two processes involved. In Fig. 13 it is proposed that the first appearance of O⁺ ions occurs at $(A_k)_{\text{min}}$ for ions of finite initial energy $(E_k)_{\text{min}}$ from the process whose dissociation limit is 18.9 ev above the ground state of NO. This appearance potential is found to be 20.6 volts (Table VII) and is lower than the 21.3 volts to be expected for ions of zero energy formed in the second process. Thus, although O⁺ ions of zero initial energy are formed in NO, the appearance potential measured for O⁺ ions cannot be attributed to them. Clearly, this can happen only when two processes having different dissociation limits are involved.

Curve 6 in Fig. 13 would lead one to expect to see a break in the O⁺ ion current curve at 21.3 ev, since it

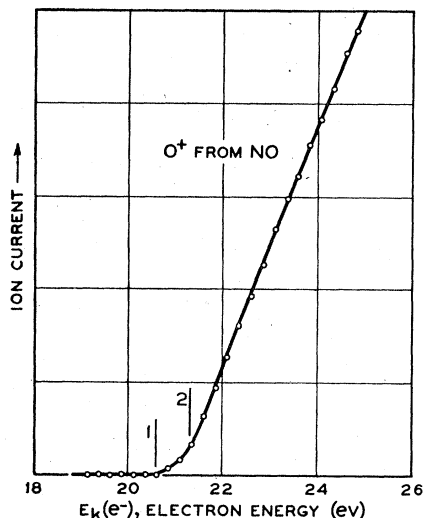


FIG. 14. O^+ ion current from dissociative ionization of NO as a function of bombarding electron energy near the appearance potential. The minimum appearance potentials of the two processes proposed in Fig. 13 are indicated at 1 and 2. Note that on the interpretation of Fig. 13 the first appearance of O^+ ions at 20.6 volts does not occur at a dissociation limit of the molecule. See text for discussion of the difficulty of observing an appearance potential such as that expected at position 2.

shows a decided step there. It should be observed, however, that curve 6 is a schematic representation of the relative probability of formation predicted by the Franck-Condon principle for transitions which take place at different nuclear separations of NO in the ground state, assuming the electronic transition probabilities about equal. The form of the O^+ ion current curve shown in Fig. 14 does not show a decided break at 21.3 eV. This perhaps means that the process yielding ions of zero energy is a less probable one. The fact that the abundance of O^+ ions of zero initial energy is only about 20 percent of that of N^+ ions of zero energy would seem to support this view. The inability to observe the second break is perhaps attributable to the background of ions from the first process. (Compare the case for O^+ ions from O_2 at 22.0 eV; see Fig. 10 and the discussion of this point in Sec. V.)

Although it cannot be said that this interpretation of the dissociative ionization processes by which O^+ is formed from NO has been proved, it appears a plausible one that accounts for all the data now available and fits nicely into the energy scheme of the molecule as determined from other more directly interpretable processes.

IX. ELECTRON CAPTURE PROCESSES YIELDING O^- IN CO, NO, AND O_2

Dissociative capture in diatomic molecules containing an electronegative atom is of particular interest because of its special properties as well as its bearing on important energies. Since the bombarding electron joins the electronic structure of the molecule to form first a

negative diatomic ion which then dissociates, its kinetic energy before impact must be in resonance with the energy transition induced in the molecule. This condition of resonance means that $\Delta E_k(e^-) = E_k(e^-)$ and that there is a one to one correspondence between $E_k(Y^-)$ and $E_k(e^-)$, expressed by the relation:

$$E_k(Y^-) = [m(X)/m(X) + m(Y^-)] \cdot [E_k(e^-) - D(XY) + EA(Y^-) - E_e(X) - E_e(Y^-)].$$

If curves 3 and 5 of Fig. 1 are now taken to refer to a molecular state of the ion XY^- dissociating to $X + Y^-$, curve 5 then represents, as for noncapture processes, the distribution in total kinetic energy of the dissociation product, as well as the relative probability of the process occurring as a function of $E_k(e^-)$. That the negative ion current does in fact show this form as a function of $E_k(e^-)$ is to be seen in Fig. 15.

The form of each resonance peak of Fig. 15 has been studied as a function of the retarding potential on the ion beam. The curves of Fig. 16 for O^- from NO taken in the manner indicated in the figure caption are typical

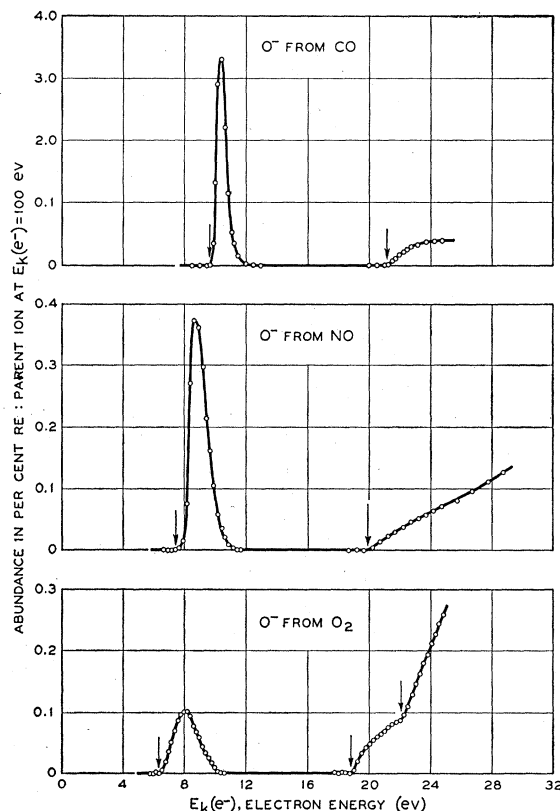


FIG. 15. Efficiency of production of O^- ions from CO, NO, and O_2 as a function of bombarding electron energy. The data at higher electron energies (Fig. 10) show the onset of processes in which a positive and negative ion are simultaneously produced [Process (B) of Table II]. The so-called resonance peaks at lower electron energies indicate the formation of ions in the capture processes [(C) of Table II] in these molecules. Note that kinetic energy measurement is essential to the interpretation of these data and the locating of dissociation limits from them (see text and Fig. 19).

of the results. As is expected, the increase in retarding potential discriminates increasingly against the ions of lower initial kinetic energy formed at lower $E_k(e^-)$. However, the curves of Fig. 16 do not merge into a single curve at higher $E_k(e^-)$ as one should expect. This is the result of velocity dispersion in the analyzer. Since the initial energy of the ions collected varies continuously across the peak, they will not be collected with equal efficiency if the total ion accelerating potential and analyzer magnetic field are kept constant. Thus, for example, in Fig. 16 the curve for $V_P=1.05$ volts, for which the analyzer was adjusted to optimum collection at $E_k(e^-)=9$ ev, lies lower at $E_k(e^-)=10$ ev than the curve for $V_P=1.45$ volts for which the analyzer had been adjusted to optimum collection at

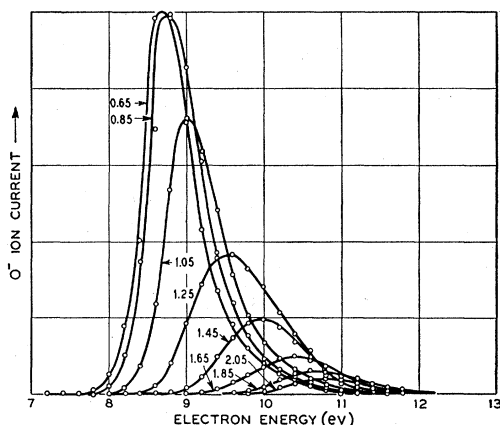


FIG. 16. Dependence of the form of the resonance peak in ionization efficiency for O⁻ from NO on retarding potential (indicated in volts for each curve). Each curve was taken with ion accelerating potential and magnetic field held constant at the values for maximum collected ion current. The effect of velocity dispersion in the magnetic analyzer is seen in the failure of the curves to merge into a single one at higher electron energies (see Fig. 17). Each curve represents the efficiency of formation of ions having kinetic energies greater than the indicated retarding potential.

$E_k(e^-)=10$ ev. When the analyzer magnetic field was adjusted to maximum ion current *at each reading*, the effect of velocity dispersion was eliminated and the data of Fig. 17 obtained. The curves of Fig. 17 for O⁻ from NO are very similar to those observed for O⁻ from O₂ and CO by Lozier³ (Figs. 2 and 7 of his paper) using retarding potentials without mass analysis. This agreement is evidence that the method of retarding potential following mass analysis in a mass spectrometer does, in fact, measure initial kinetic energies in a manner strictly comparable to Lozier's method in which the ions are formed in a field free region.

The initial portions of the curves of Fig. 17 are replotted in Fig. 18, in which is also indicated the assignment of appearance potentials. For retarding potentials less than 0.65 volt the curves (not shown) fall very closely upon one another as all ions are then collected.

In Fig. 19 the appearance potential *versus* retarding potential data obtained from curves like those of Fig. 18

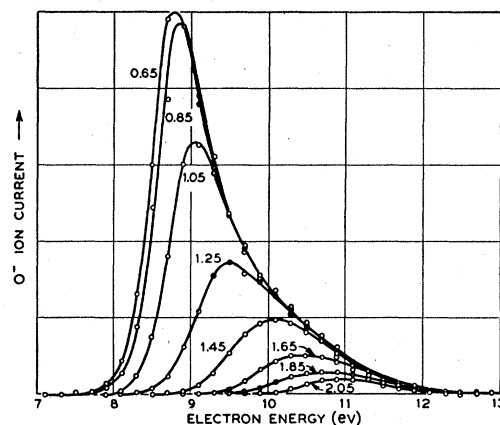


FIG. 17. Efficiency of formation of O⁻ ions from NO taken for several values of retarding potential (indicated in volts for each curve), the magnetic analyzing field being adjusted at each point to maximum collected ion current. This procedure has eliminated the effect of velocity dispersion in the analyzer evident in the curves of Fig. 16.

are plotted for O⁻ ions from CO, NO, and O₂. In obtaining these data, the kinetic energy scale is calibrated by ions of zero initial energy formed in the process of type (B) at $E_k(e^-)=60$ ev (Sec. IV). Since this determination involves a large change in $E_k(e^-)$ in addition to a change in m/e , it is necessary to check it in some way. In Sec. IV it was reported that the retarding potential curve of an ion known to be formed at rest shifted by more than 0.2 ev when $E_k(e^-)$ was varied from 30 to

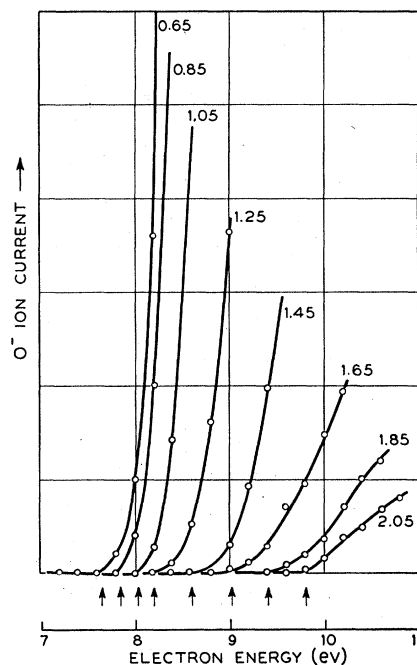


FIG. 18. Appearance potential data for O⁻ ions from process (C) in NO having various initial kinetic energies [indicated in volts for each curve]. These are the initial portions of the resonance peaks plotted in Fig. 17. The appearance potentials indicated by the arrows below the curves are used in Fig. 19.

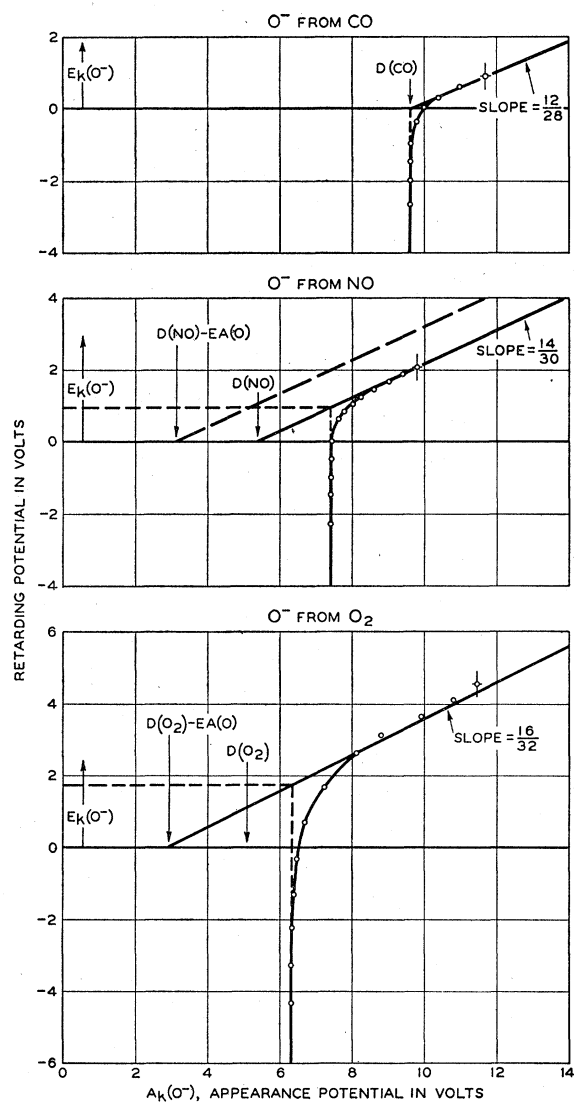


FIG. 19. Plots of retarding potential vs appearance potential for O^- ions from the resonance capture processes in CO, NO, and O_2 . Data are given for retardation between electrodes N and P (region of E_k, A_k plot) and for acceleration between N and P (negative retarding potential, all ions collected at P). Possible experimental error is indicated at the datum point at highest A_k for each curve. The intercept on the A_k axis, locating the dissociation limit of the process, is interpreted in each case as indicated. The dashed E_k, A_k line of slope $14/30$ for O^- (NO) is for the dissociative capture process observed by Hanson (see text).

100 ev. Furthermore, it is not possible to extend this measurement down to the range of electron energies in which the dissociative capture processes occur. One can perform an independent check of the results, however, by comparing the results for O^- from dissociative capture in CO with Lozier's³ measurements. This check, together with the internal consistency of the data, shows the method to introduce only slightly greater error than that used for other ions. The possible experimental error is indicated at the "top" datum point of

each plot in Fig. 19. The electron energy scale in these measurements was calibrated directly against the appearance potential of O^- ions from the process (B) which, in turn, had been checked against $A(Ne^+)$. The measurement of appearance potentials for ions having appreciable kinetic energies from dissociative capture was found to be much easier than that for $O^+(CO)$ because of the resonance nature of the process and the consequent "sudden" appearance of the ion as electron energy is raised.

The vertical line upon which the data points lie at negative retarding potentials in Fig. 19 (acceleration of the ions between electrodes N and P) indicates the minimum value of $A_k(O^-)$ for ions of least initial energy. Since all ions are collected, this appearance potential should be independent of the amount of acceleration of the ions between N and P . In the region of positive retarding potentials, the retarding potential determines the minimum kinetic energy of the ions striking electrode P . In this region the data lie on a straight line of proper slope and form an E_k, A_k plot like those of Fig. 2. The rounding off of the corner at the intersection of the two lines is undoubtedly instrumental in origin. A similar effect is to be noted in Lozier's data (his Fig. 3).³ Of particular interest is the fact that this intersection, indicating the point of minimum $E_k(O^-)$ and minimum $A_k(O^-)$, falls on the $E_k(O^-)=0$ line only for O^- from CO. Thus, for this case only are ions of zero initial kinetic energy formed. For O^- from NO and O_2 the minimum kinetic energies are indicated by the horizontal dashed lines in Fig. 19. They are recorded in Table VII.

The kinetic energy corresponding to the highest lying datum point on each curve in Fig. 19 gives some indication of the maximum kinetic energy observed in each process. Beyond this point the intensity was found to be so low that it made a reliable measurement impossible (Fig. 2). Thus, O^- ions of energies greater than about 1, 2.5, and 5 volts in CO, NO, and O_2 respectively, are not formed with any appreciable abundance. These conclusions concerning the bounds on ion kinetic energies are in reasonable agreement with the kinetic energies for these ions observed by Lozier³ and Hanson.⁴

The extension of the E_k, A_k line to $E_k(O^-)=0$ gives $A_0(O^-)$, the level of the dissociation limit. These values are included in Tables IV and V. From the expression for A_0 in Table II for these processes [type (C)] the values of $D(XY)$ listed in Table VI have been calculated [second column under (C) for NO and first for O_2]. The value which agrees with that from the other dissociative ionization processes dictates the interpretation of the process given in Table V. The interpretations of the A_0 values as $D(CO)$, $D(NO)$, and $D(O_2)-EA(O)$ for O^- ions from CO, NO, and O_2 , respectively, are indicated in Fig. 19.

Hanson,⁴ in his work on NO, observed ions from a process having $A_0=D(NO)-EA(O)$, his data points lying along the dashed line through this point indicated

in Fig. 19. Since he complains of low intensity with an apparatus conservatively estimated to have 1000 times the collection sensitivity of that used in this work, ions from this process could not possibly have been observed with the present instrument. The onset for the second process having $A_0=5.3$ volts was not looked for by Hanson. Thus, two resonance capture processes yielding O⁻ ions have been observed in NO (Table V). Lozier observed a second process in O₂ having $A_0=12.0$ volts (Table V), which was not observed in the present work. All these resonance capture processes fit well into the energy level scheme as Tables V and VI indicate.

The E_k, A_k curves of Fig. 19 have been obtained from appearance potential data obtained by varying the electron energy at constant retarding potential (Fig. 18). One can for these resonance processes in effect reverse this procedure and obtain the data from retarding potential curves taken at constant electron energy, $E_k(e^-)$. In Fig. 20 (top) are plotted such data for O⁻ ions from dissociative capture in O₂ at $E_k(e^-)=7.5, 8.5,$ and 9.5 ev as well as for O⁻ ions from process (B) in O₂ at $E_k(e^-)=60$ ev.

Since ions of zero initial energy are formed in process (B), the point of maximum slope for $E_k(e^-)=60$ ev in Fig. 20 should define the zero point on the kinetic energy scale [Fig. 6 (b)]. For a given $E_k(e^-)$ all the ions from the dissociative capture process, on the other hand, possess the same kinetic energy. One could determine this energy as discussed in Sec. IV by noting the displacement along the retarding potential scale of the point of maximum slope from that for $E_k(e^-)=60$ ev. A second method of calibrating the kinetic energy scale is used in Fig. 20, however. The retarding potential curve for an ion formed at rest [Fig. 6(a)] is fitted to the top part of the O⁻ curve for $E_k(e^-)=60$ ev (dashed line in Fig. 20). The point on the abscissa scale at which the ordinate of this curve vanishes is the maximum retarding potential at which ions of zero initial energy can be observed. If this point is taken to define the zero of kinetic energy, the vanishing points of the curves for ions from dissociative capture then gives the corresponding kinetic energies. The two methods of calibrating the kinetic energy scale discussed above give values of $E_k(O^-)$ for the ions from dissociative capture within experimental error.

The $E_k(O^-), A_k(O^-)[=E_k(e^-)]$ values obtained in this way are plotted in Fig. 20 (bottom), giving a curve in agreement with that of Fig. 19. Similar data have been obtained for O⁻ from CO and NO.

X. DISSOCIATION ENERGY OF CO AND SUBLIMATION ENERGY OF C

In this and the succeeding three sections of this paper will be discussed the important energies for which these electron impact experiments yield specific values. No attempt is made to discuss or evaluate all the work bearing on these quantities. Rather, the discussion

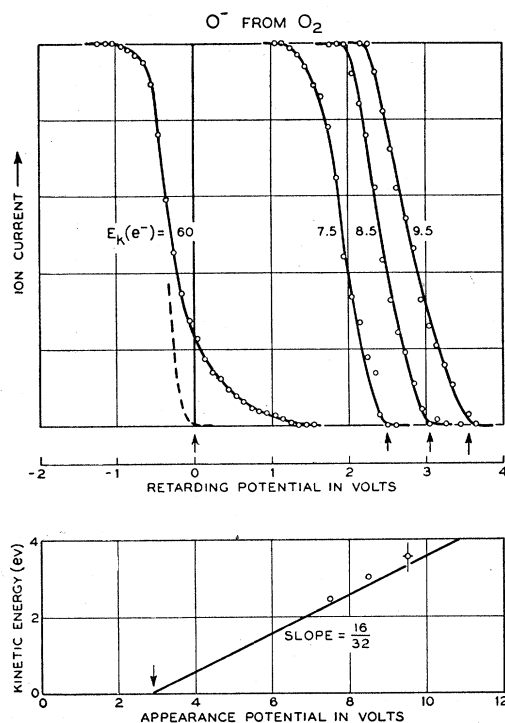


FIG. 20. *Top*: Retarding potential curves for O⁻ ions from the resonance capture process in O₂ measured at constant $E_k(e^-)$ (indicated in volts at each curve). The position of the curve for ions from process (B) formed at $E_k(e^-)=60$ v is used to calibrate the retarding potential scale as indicated in the text. Retarding potentials for first appearance of ions of specified E_k are indicated by arrows on the retarding potential scale. *Bottom*: Plot of retarding potentials [$E_k(O^-)$] vs electron energies [$A_k(O^-)$] obtained from the curves in the top graph. The E_k, A_k line of proper slope is drawn through the point $A_0=2.9$ v. The possible experimental errors in these data are indicated at the datum point of highest A_k .

here will comprise a statement of what might be called the "electron impact position" with regard to them, and some mention of other work not already discussed.^{6,10,25}

The electron impact value for $D(\text{CO})$ rests upon the measurement of appearance potentials and kinetic energies of ions formed in the four dissociative ionization processes observed in CO listed in Table V. These lead as Table VI indicates to the single value of 9.6 ev for $D(\text{CO})$ in agreement with the spectroscopic value of 9.605 ev.¹⁰ It is difficult to see how one could reinterpret these electron impact data to bring agreement with any other value of $D(\text{CO})$ without doing considerable violence to a set of data for the molecules CO, N₂, NO, O₂, and H₂, which is not only internally consistent but agrees within limit of experimental error with spectroscopic values wherever they are available. This implies no blanket claim of accuracy for all appearance potentials which have been measured by electron impact, however.

Since this writer's review of work bearing on $D(\text{CO})$

²⁵ H. D. Hagstrum, J. Chem. Phys. 16, 848 (1948).

and $L_1(\text{C})$,¹⁰ several investigations generally favorable to a value of $D(\text{CO})$ near 9.6 ev have been reported.²⁶⁻²⁸ However, recent measurements^{29,30} of the vapor pressure of carbon as a function of temperature have been taken to support the highest spectroscopic value, 11.108 ev, advocated in recent years.³¹ This might tempt one to interpret processes (A), (B), and (C) in CO (Table V) as yielding unexcited products and ascribe the difference between the values of $D(\text{CO})$ calculated from the appearance potentials (Table VI) to experimental error. Beyond the fact that the 0.5- to 0.7-ev error it is necessary to assume appears to be beyond reason in the light of the apparent quality of the electron impact data, one encounters a flat contradiction for process (A'). For it, $A_0 = 23.2 \pm 0.3$ ev gives for unexcited products the maximum permissible value of $D(\text{CO}) = 9.6 \pm 0.3$ ev. The fact that the interpretation of many electron impact processes require excited products is not too surprising when one considers the rather stringent requirements placed by the Franck-Condon principle on the position of the upper potential curve if dissociative ionization involving the curve is to be observed. This writer concurs in the opinion that the experimental difficulty of the high temperature work with carbon and the fact that an accommodation coefficient near unity has by no means been demonstrated make the vapor pressure results less reliable than those obtained by electron impact.³² Finally, it should be noted that from further electron impact work in CH_4 , McDowell and Warren³³ conclude that $L_1(\text{C})$ cannot possibly be greater than 140 kcal/mole (which corresponds closely to $D(\text{CO}) = 9.6$ ev). The electron impact experiments thus seem to indicate strongly that $D(\text{CO}) = 9.605$ ev ($77,500 \text{ cm}^{-1}$); $L_1(\text{C}) = 5.887$ ev [135.7 kcal]; $L_2(\text{C}) = 10.07$ ev [232.1 kcal]; $D(\text{CO}^+) = 6.8$ ev; and $D(\text{CN}) = 6.43$ ev.

²⁶ H. G. Howell, *Nature* **163**, 773 (1949) [determination by a short extrapolation of vibrational levels of the dissociation limit of the F^{II} state of CO yielding $D(\text{CO}) = 9.6$ ev].

²⁷ L. H. Long, *Proc. Roy. Soc. (London)* **A198**, 62 (1949) [evidence from the heats of formation of free CN and free CH_2 and the relationship among $D(\text{CO})$, $D(\text{CN})$, and $D(\text{N}_2)$].

²⁸ L. Pauling and W. F. Sheehan, Jr., *Proc. Natl. Acad. Sci. (U. S.)* **359** (1949) [a novel use of linear extrapolation of vibrational states and the hypothetical valence state leading to $D(\text{CO}) = 9.77$ ev].

²⁹ Brewer, Gilles, and Jenkins, *J. Chem. Phys.* **16**, 797 (1948).

³⁰ A. L. Marshall and F. J. Norton, *J. Am. Chem. Soc.* **72**, 2166 (1950).

³¹ A. G. Gaydon, who had favored $D(\text{CO}) = 11.108$ ev on the basis of the noncrossing rule [*Dissociation Energies and Spectra of Diatomic Molecules* (John Wiley and Sons, Inc., New York, 1947), p. 169 ff.] now seems willing to accept a lower value [*Nature* **163**, 773 (1949); *Spectroscopy and Combustion Theory* (Chapman and Hall, London, 1948), second edition, p. 190].

³² See comments of L. H. Long, *Proc. Roy. Soc. (London)* **A198**, 62 (1949), p. 71 ff. Note also Brewer's answer [*J. Chem. Phys.* **16**, 1165 (1948)] to Long's earlier comments [*J. Chem. Phys.* **16**, 1087 (1948)].

³³ C. A. McDowell and J. W. Warren's work is referred to by H. D. Springall in a note added in proof to his review of work on the heat of atomization of carbon [*Research* **3**, 206 (1950)]. See also the recent calculation of F. H. Field [*J. Chem. Phys.* **19**, 793 (1951)], which, using published appearance and ionization potential data for fragments from methane, yields $L_1(\text{C})$ in the neighborhood of 136 kcal/mole.

XI. DISSOCIATION ENERGIES OF N_2 AND NO

The possible values of $D(\text{N}_2)$ and $D(\text{NO})$ from the electron collision experiments are also given in Table VI. Although the onset potential of the single dissociative ionization process in N_2 cannot yield a unique value for $D(\text{N}_2)$, it does decide against the 8.565-ev value now also eliminated by band spectroscopy.³⁴ $D(\text{N}_2)$ is determined, however, by its relation to $D(\text{NO})$ through $D(\text{O}_2)$ and the known heat of formation of NO. The electron impact results for NO fix $D(\text{NO}) = 5.3$ ev as Table VI demonstrates and thus select for $D(\text{N}_2)$ the 7.373-ev value.³⁵

Here as for CO it is extremely difficult to see how one can give the electron impact data any other interpretation than that presented. Note the excellent numerical agreement of the dissociation limits from appearance and retarding potential data both in N_2 and NO with the predissociation limits at 97,944 and 78,843 cm^{-1} in N_2 .³⁴ Thus, the electron collision data support the values $D(\text{N}_2) = 7.373$ ev and $D(\text{NO}) = 5.296$ ev.

XII. ELECTRON AFFINITY OF O

The electron affinity of oxygen is determined directly in the electron impact experiments by the location of the dissociation limits for the capture processes $\text{NO} \rightarrow \text{N}(^4S^0) + \text{O}^-(^2P^0)$, $\text{O}_2 \rightarrow \text{O}(^3P) + \text{O}^-(^2P^0)$, and $\text{O}_2 \rightarrow \text{O}^*(^5S^0) + \text{O}^-(^2P^0)$ at 3.2, 2.9, and 12.0 ev, respectively (Tables IV and V). These yield the value $EA(\text{O}) = 2.2 \pm 0.2$ ev. Other choices of excitation of the products lead to clearly impossible values for $EA(\text{O})$. Furthermore, the excellent agreement with the 2.33-ev value from the study of electron attachment at a hot filament³⁶ makes it appear quite certain that $EA(\text{O}) = 2.2 \pm 0.2$ ev.

In all other processes involving the O^- ion in CO, NO, and O_2 the ion is formed in an excited state [Sec. XIII].

XIII. EXCITED STATE OF O^-

In six of the nine processes in which O^- ions are formed from CO, NO, and O_2 , the appearance potential for ions of zero initial kinetic energy, A_0 , demands that $E_a(\text{O}^-) = EA(\text{O})$ (Table V).³⁷ The processes commence at electron energies to be expected for unexcited O atoms rather than the O^- ions observed. This equality

³⁴ A. E. Douglas and G. Herzberg [*Can. J. Phys.* **29**, 294 (1951)] report finding a predissociation above $v' = 6$, $J' = 13$ in a $^1\Pi_g$ at $78,843 \pm 50 \text{ cm}^{-1}$, which, together with the limit at $97,944 \text{ cm}^{-1}$ in $v' = 2, 3$, and 4 of $\text{C}^3\Pi_u$, makes $D(\text{N}_2) = 8.565$ ev impossible.

³⁵ The value $D(\text{N}_2) = 11.80$ ev proposed by G. Glockler [*J. Chem. Phys.* **19**, 124 (1951)] on the basis of estimates and interpolations must be rejected. The process in N_2 commencing at 24.3 ev cannot yield $\text{N}^+ + \text{N}^-$ as Glockler suggests because N^- ions have not been observed even though they should appear in numbers equal to the N^+ . Thus, the maximum value of $D(\text{N}_2)$ from the electron impact datum in N_2 alone is 9.8 ev (Table VI).

³⁶ M. Metlay and G. E. Kimball, *J. Chem. Phys.* **16**, 774 (1948).

³⁷ A possible alternative interpretation of the second process (C) in NO (given in brackets in Table V) would excite the \tilde{N} atom rather than the O^- ion. Better numerical agreement with the other data is obtained for the first interpretation, however.

of excitation energy and electron affinity means that the extra electron is very loosely bound to the O atom, $E_a(O^-) \cong 2.2$ ev. Thus, the O^- excited state observed here is that which lies very close to the positive energy continuum, the only stable excited state considered possible on theoretical grounds.³⁸ With one possible exception,³⁷ placing of the 2.2-ev excitation on the other

product in these six processes is clearly impossible within limits of experimental error.

The author wishes to express his gratitude to P. W. Anderson, G. H. Wannier, and A. H. White for helpful discussions during the course of the work; to P. W. Anderson, R. E. Fox, N. B. Hannay, and T. Kjeldaaas for critical reading of the manuscript; to H. W. Weinhart, under whose supervision the experimental tube was constructed; and to F. J. Koch for technical assistance.

³⁸ H. S. W. Massey, *Negative Ions* (Cambridge University Press, London, 1950), second edition, p. 20.

The Copper Oxide Rectifier

WALTER H. BRATTAIN

Bell Telephone Laboratories, Murray Hill, New Jersey

It is shown that the conductivity in the ohmic part of the cuprous oxide layer can be explained with the usual band picture of semiconductors only by assuming the presence of some donor-type impurities in addition to the usual acceptor type. The energy difference between the acceptors and the filled band is 0.3 electron volt, and the total number of impurity atoms is about 10^{14} to 10^{16} per cm^3 , the number of donors being less than but of the same order as the number of acceptors. Applying the Schottky theory of the space charge exhaustion layer, one finds from the dependence of capacity of the rectifier on bias voltage that the density of ion charge in the rectifying layer is of the same order of magnitude as the difference between the donors and acceptors found from the conductivity, thus furnishing a check for the theory. The field at the copper-cuprous oxide interface calculated from the space charge is about 2×10^4 volts/cm; the height of the potential at the surface as compared with the oxide interior is about 0.5 volt; and the thickness of the space charge layer about 5.0×10^{-5} cm. The diffusion equation for flow of current through this space charge region can be integrated to give the current in terms of the field at the interface and the applied potential across the space

charge layer. Two currents are involved, one from the semiconductor to the metal (I_s) and one from the metal to the semiconductor (I_m) which is similar to a thermionic emission current into the semiconductor. The net current is, of course, $I = I_m - I_s$. One can get this "emission" current (I_m) by dividing the true current by the factor $1 - \exp(-eV_a/kT)$, where V_a is the applied potential. This emission current depends on the absolute temperature and on the field at the copper-cuprous oxide interface. At high fields the logarithm of the current is proportional to the square root of the field, and at low fields the current decreases more rapidly indicating a patchy surface having small areas of low potential maximum from which all the emission comes when the field is large. This effective potential maximum measured from the Fermi level in the copper is about 0.5 ev, and the fraction of the total area effective ranges from 10^{-2} to 10^{-5} depending on how the rectifier was made. This last factor—the fraction of the area having this low potential maximum—is by far the most important variable, resulting in low reverse currents when the fraction is small and large reverse currents when the fraction is large.

I. INTRODUCTION

DURING the past few years considerable progress has been made toward an understanding of rectification at a metal-semiconductor contact. Mott¹ has shown that rectification results from a potential barrier at the contact which impedes the flow of current carriers, electrons or holes. The width of the barrier is so large, 1000 Å or more, that tunneling is relatively unimportant. Electrons must have sufficient thermal energy to surmount the barrier.

Schottky² has shown that this barrier, or blocking layer, may be physical rather than chemical in nature. In a physical blocking layer the potential barrier results from a space charge layer in the semiconductor next to the metal and the corresponding induced charge on the metal surface. These two charge distributions form a

double layer which adjusts the potential of the semiconductor relative to the metal for equilibrium conditions. The space charge arises from ionized impurity centers. These centers are of the same nature, and may even have the same concentration, as those responsible for the conductivity in the main body of the semiconductor. No change in the chemical constitution of the semiconductor next to the metal is required. If the impurity centers are completely ionized throughout most of the barrier region, Schottky's exhaustion layer theory may be applied. The theory is much simplified for this limiting case, which is the most important one for practical applications.

Mott applied his theory to the copper oxide rectifier. Schottky used the selenium rectifier as his primary example, and he also discussed briefly the application to copper oxide. During the war there was a good deal of work done in this country on the theory of the point

¹ N. F. Mott, Proc. Roy. Soc. (London) **171**, 27 (1939).

² W. Schottky, Z. Physik **113**, 367 (1939).